Compositional phase stability of strongly correlated electron materials within DFT+U

Eric B. Isaacs* and Chris A. Marianetti†
Department of Applied Physics and Applied Mathematics, Columbia University, New York, NY 10027
(Dated: November 14, 2016)

Predicting the compositional phase stability of strongly correlated electron materials is an outstanding challenge in condensed matter physics. In this work, we employ the density functional theory plus U (DFT+U) formalism to address the effects of local correlations due to transition metal d electrons on compositional phase stability in the prototype phase stable and separating materials Li_xCoO_2 and olivine Li_xFePO_4, respectively. We exploit a new spectral decomposition of the DFT+U total energy, revealing the distinct roles of the filling and ordering of the d orbital correlated subspace. The on-site interaction U drives both of these very different materials systems towards phase separation, stemming from enhanced ordering of the d orbital occupancies in the $x = 0$ and $x = 1$ species, whereas changes in the overall filling of the d shell contribute negligibly. We show that DFT+U formation energies are qualitatively consistent with experiments for phase stable Li_xCoO_2, phase separating Li_xFePO_4, and phase stable Li_xCoPO_4. However, we find that charge ordering plays a critical role in the energetics at intermediate x, strongly dampening the tendency for the Hubbard U to drive phase separation. Most relevantly, the phase stability of $Li_{1/2}CoO_2$ within DFT+U is qualitatively incorrect without allowing charge ordering, which is problematic given that neither charge ordering nor the band gap that it induces are observed in experiment. We demonstrate that charge ordering arises from the correlated subspace interaction energy as opposed to the double counting. Additionally, we predict the Li order-disorder transition temperature for $Li_{1/2}CoO_2$, demonstrating that the unphysical charge ordering within DFT+U renders the method problematic, often producing unrealistically large results. Our findings motivate the need for other advanced techniques, such as DFT plus dynamical mean-field theory, for total energies in strongly correlated materials.

PACS numbers: 71.15.Mb, 71.27.+a, 81.30.Bx, 82.47.Aa

arXiv:1611.03517v1 [cond-mat.str-el] 10 Nov 2016

I. INTRODUCTION

Strongly correlated materials (SCMs), in which density functional theory (DFT)[1,2] calculations break down for selected observables due to strong electron-electron interactions, are at the forefront of condensed matter physics.[3,4] Phenomenologically, SCMs exist in a ground state which is in the vicinity of a Mott transition[5,6] whereby electronic hopping may be overwhelmed by local interactions, resulting in an insulating state. Realizations of SCMs often contain atoms with open-shell d or f electrons, such as the high-temperature superconducting cuprates[7], colossal magnetoresistance manganites[8], and heavy fermion actinide based materials.[9]

Predicting the properties of strongly correlated materials is an outstanding problem in solid state physics. The standard approach of DFT, which is the most generic theory of electronic structure for materials physics, is in principle an exact theory for the ground state energy and electron density of any many-electron system. However, the exact exchange-correlation functional is unknown and must be approximated; and in practice DFT is often unable to capture critical aspects of the physics of strongly correlated materials.[3,10,11] The difficulty of constructing increasingly intelligent exchange-correlation density functionals led to pursuit of additional variables that could be more easily approximated; one such variable is the local Green function for a set of correlated orbitals in the material (e.g d orbitals)[12]. A corresponding approximation for this density plus local Green functional theory leads to DFT plus dynamical mean-field theory (DFT+DMFT). A further Hartree approximation to the DMFT impurity problem leads to the more ubiquitous DFT+U approach, which can be counterintuitive given that the latter preceded the former historically[12,13]. The long-term goal of these techniques is their application in an unbiased manner to any material containing localized orbitals, nominally or otherwise. Compositional phase stability is a particular stringent test since it relies on total energies from multiple compositions, making it more difficult to cancel errors by varying the few still maturing aspects of the formalism.

One of many important contexts highlighting the need for accurate total energy methods for strongly correlated materials is that of doped transition metal oxides, which include doped Mott insulators. From a technological perspective, Li-based transition metal oxides form the basis of rechargeable battery cathodes. Such cathodes typically employ transition metals and oxygen or oxygen-containing anion groups and, since they have open d electron shells, are susceptible to strong correlation physics. One fundamental characteristic of a cathode material is whether there is a stable solid solution for intermediate Li concentration ($0 < x < 1$), as dictated by the formation energy of the compound. The formation energy has a strong impact on the charge/discharge mechanism and also has implications for the voltage and capacity of the battery.

Many of the current cathode materials utilized today are based on the material Li_xCoO_2, shown in Fig.

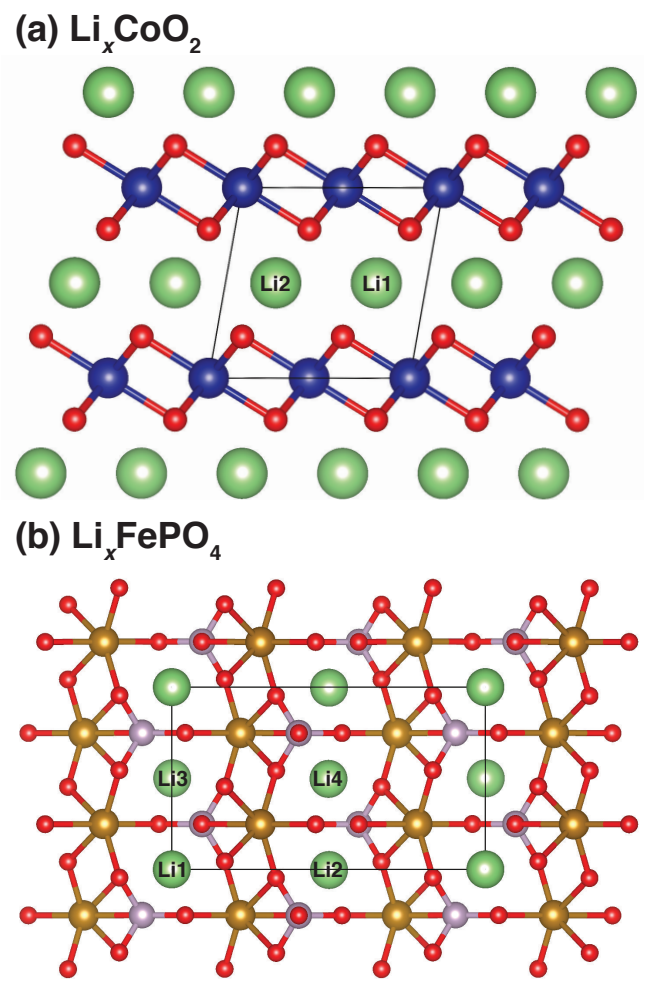

FIG. 1. Crystal structures of (a) Li_xCoO_2 and (b) Li_xFePO_4. The large green, medium blue, medium gold, small purple, and small red spheres represent ionic positions of Li, Co, Fe, P, and O, respectively. The black lines indicate for (a) the unit cell of the lowest-energy $Li_{1/2}CoO_2$ configuration and for (b) the primitive unit cell. Images of crystal structures are generated using VESTA.[14]

1(a) for $x = 1$, which can store Li ions in between its CoO_2 layers.[15] Li_xCoO_2 has several stable intermediate phases.[16–18] In contrast, olivine Li_xFePO_4[19,20] [see Fig. 1(b)] does not have any stable compounds for intermediate x. It instead exhibits phase separation into its fully lithiated ($x = 0$) and fully delithiated ($x = 1$) endmembers, which may contribute to slow charge/discharge kinetics.[19,21,22]

Previous work demonstrates that DFT predicts very stable compounds of intermediate x in Li_xFePO_4, in stark disagreement with experiment.[23] This is a flagrant failure of the DFT method. In contrast, DFT does properly capture the phase stability of Li_xCoO_2.[17,18] A beyond-DFT approach combining DFT and Hartree-Fock exchange, called a hybrid functional, also fails to capture the total phase separation in Li_xFePO_4.[24] DFT+U calculations, which include an explicit on-site Coulomb interaction U for the transition metal d electrons, were found to predict phase separation in Li_xFePO_4 for sufficiently high values of U.[23] In later work, a cluster expansion based on such DFT+U energetics rationalized this phase separation in terms of strong Li–electron interactions.[25] A lingering question, which we will address in this work, is whether DFT+U can be applied to Li_xCoO_2[26–29] without degrading the already reasonable DFT results, such that DFT+U can give a robust description for both of these prototype phase stable and phase separating systems.

The DFT+U study for Li_xFePO_4 claims that the instability of compounds of intermediate x relates to energy penalties stemming from charge ordering (CO), a symmetry breaking in which the number of electrons on different transition metal sites differs.[23] However, it is unclear if the CO is physical since static ordering is the only way in which a static mean-field theory like DFT+U can mimic strong electronic correlations. Furthermore, the phase separation in Li_xFePO_4 is fundamentally puzzling since with reasonable parameters the canonical model Hamiltonians describing strong correlations such as the Hubbard and t–J models do not exhibit phase separation for extended regions of the phase diagram.[30,31]

To explore such issues, in this work we employ extensive DFT+U calculations to understand in detail the impact of electronic correlations on phase stability in correlated intercalation materials. We focus on phase stable Li_xCoO_2 and phase separating Li_xFePO_4 and explicitly investigate the role of CO and structural relaxations. A new energy decomposition is elucidated to quantitatively analyze the impact of U on the overall filling and on the ordering of orbitals within the d shell. Comparison is made to the Li_xCoPO_4 system, which is isostructural to Li_xFePO_4 but does have a stable compound of intermediate x. We also investigate another physical observable, the Li order-disorder transition temperature, for $Li_{1/2}CoO_2$ to provide another clear benchmark of DFT+U theory. The tendency for CO in DFT+U, how it impacts these thermodynamic properties, and whether it is physical or not is investigated and discussed. A thorough understanding at the DFT+U level of theory is critical as we advance to more sophisticated methods for studying phase stability in strongly correlated materials.

For all the materials we have investigated, we find that U destabilizes compositions at intermediate x. This results because U most strongly affects the endmembers by enhancing the deviations in the d orbital occupancies from their average value; compounds of intermediate x experience the same effect but are unable to orbitally polarize to the same extent, which directly drives them towards phase separation as U increases. CO and structural relaxations serve to dampen, but not eliminate, this fundamental effect. However, CO leads to the formation of a band gap for $Li_{1/2}CoO_2$ that is not observed ex-

perimentally, suggesting it is an unphysical artifact of DFT+U. Furthermore, CO leads to highly erratic estimations of the Li order-disorder transition temperature for $Li_{1/2}CoO_2$, demonstrating a serious shortcoming of the DFT+U method. Our calculations demonstrate that the interaction term rather than the double counting term in DFT+U is responsible for the CO, which suggests that more accurate approaches such as DFT plus dynamical mean-field theory (DFT+DMFT) may be necessary to accurately describe this class of materials.

The rest of this paper is organized as follows. Section II discusses the DFT+U approach to materials with strong electronic correlations and elucidates our new energy decomposition in this framework. Section III describes the computational details for the simulations performed in this work. The electronic structure of the endmembers of Li_xCoO_2 and Li_xFePO_4 within DFT are described in Sec. IV A. The impact of U on the electronic structure of Li_xCoO_2 is discussed in Sec. IV B. The origin of the tendency for CO in DFT+U, taking Li_xCoO_2 as an example, is the focus of Sec. IV C. The impact of U on the phase stability of Li_xCoO_2 is discussed in Sec. IV D. The electronic structure and phase stability of Li_xFePO_4 within DFT+U are described in Sec. IV E and Sec. IV F, respectively. Section IV G discusses the formation energy trends for Li_xCoPO_4. Section IV H elucidates the role of the double counting on the formation energy trends. The average intercalation voltages for Li_xCoO_2 and Li_xFePO_4 are presented in Sec. IV I. Section IV J focuses on the Li order-disorder transition temperature of $Li_{1/2}CoO_2$ and its dependence on CO. Finally, conclusions are presented in Sec. V.

II. METHODOLOGY

A. DFT+U approach for correlated materials

The idea of DFT+U[32] is to provide an improved treatment of electronic correlations by using not only the density ρ as a primary variable of the energy functional, but also the single-particle density matrix of a relevant set of local orbitals associated with strong correlations. This set of orbitals, which form the correlated subspace, are typically localized electronic states having d or f character and in practice are defined using Wannier functions or atomic orbitals $|\phi^\tau_m\rangle$ labeled by ionic site τ and angular momentum projection m.

Having defined the correlated subspace, one needs to construct an approximation for the energy as a functional of the density and the single-particle density matrix of the correlated subspace. This is typically approximated using two separate additive functionals:

$$E_{\mathrm{DFT}+U}[\rho, n^{\tau s}] = E_{\mathrm{DFT}}[\rho] + E_U[n^{\tau s}] - E_{\mathrm{dc}}[n^{\tau s}]. \quad (1)$$

where $n^{\tau s}$ is the local single-particle density matrix for spin projection s and $E_{\mathrm{DFT}}[\rho]$ is the usual Kohn-Sham DFT energy functional using one of the many possible approximations to the exchange-correlation energy such as the local density approximation (LDA)[33–36] or the generalized gradient approximation (GGA).[37,38] The functional of the density matrix $E_U[n^{\tau s}]$, to be defined mathematically below, is given by the Hartree-Fock interaction energy based upon a set of screened interactions within the correlated subspace. There is a clear double counting (dc) problem with such a formulation, as the LDA or GGA already accounts for some interactions of the density arising from the correlated subspace, and therefore a double-counting energy $E_{\mathrm{dc}}[n^{\tau s}]$ must be defined and subtracted.

It is common to employ the spin-dependent formulation of DFT (SDFT) rather than pure DFT, in which case the total energy expression becomes

$$E_{\mathrm{SDFT}+U}[\rho^s, n^{\tau s}] = E_{\mathrm{SDFT}}[\rho^s] + E_U[n^{\tau s}] - E_{\mathrm{dc}}[n^{\tau s}], \quad (2)$$

where ρ^s is the density for spin projection s. In the simplified rotationally-invariant formalism of Dudarev *et al.*[39] the interaction term, which we always write in the diagonal eigenbasis of the density matrix, is

$$E_U[n^{\tau s}] = \frac{1}{2}U \sum_{\tau, ms \neq m's'} n^{\tau s}_m n^{\tau s'}_{m'}, \quad (3)$$

where $n^{\tau s}_m$ is the mth eigenvalue of $n^{\tau s}$ and U represents the screened on-site Coulomb energy between different spin-orbitals within the correlated subspace. This approach is equivalent to the full rotationally-invariant formalism by Liechtenstein *et al.*[40] if the on-site exchange parameter J is set to 0, which can be justified by previous work indicating that SDFT already contains an intrinsic J.[41,42] The most commonly used dc is the fully-localized-limit (FLL) type

$$E_{\mathrm{dc}}[n^{\tau s}] = \frac{1}{2}U \sum_\tau N^\tau (N^\tau - 1), \quad (4)$$

in which $N^\tau = \sum_{m,s} n^{\tau s}_m$ is the total correlated occupancy on a site. In this work we focus on materials in which d states form the correlated subspace, so at times we refer to this quantity as N^τ_d (or N_d if there is only a single site). This double counting energy is equal to $E_U[n^{\tau s}]$ in the limit in which all $n^{\tau s}_m$ take on values of 0 or 1.

Using this dc form, the total energy expression can be rewritten as

$$E_{\mathrm{SDFT}+U}[\rho^s, n^{\tau s}] = E_{\mathrm{SDFT}}[\rho^s] + \frac{1}{2}U \sum_{\tau, m, s} n^{\tau s}_m (1 - n^{\tau s}_m). \quad (5)$$

This form illustrates that DFT+U penalizes fractional occupancy of the correlated orbitals and serves to restore the derivative discontinuity of the total energy with respect to total particle number that is missing in approximate DFT.[32,43–45]

It is important to emphasize the connection between DFT+U and DFT+DMFT to in order to appreciate the limitations of the DFT+U approach.[12] DFT+DMFT corresponds to a functional of the density and the local Green function of the correlated orbitals, which contains the single-particle density matrix in addition to information about single-particle excitations. This functional is approximated using, in part, DMFT, which requires the solution of the DMFT impurity problem. Since the DMFT impurity problem itself is a difficult (though tractable) many-body problem, one approach is to make further approximations and solve the DMFT impurity problem within the Hartree-Fock approximation, which results in the DFT+U approach. Alternatively, it may be possible to exactly solve the DMFT impurity problem using quantum Monte Carlo (QMC) techniques[46,47], which can have a profound influence on the energetics as compared to DFT+U[41,48,49]. In particular, the error associated with DFT+U was shown to strongly depend on the spin state of Fe in a spin crossover molecule[41], which may suggest that DFT+U errors will strongly depend on Li concentration in cathode materials and therefore affect phase stability and battery voltages. The quality of DFT+DMFT (solved using QMC) is superior to DFT+U in every sense, but the former is far more computationally expensive and complex. This current study will give us a detailed understanding of how DFT+U performs in the context of phase stability, sometimes exposing obvious deficiencies but also demonstrating enhancements over DFT, and provide a baseline on which DFT+DMFT may improve. A forthcoming publication will then extend the current study using DFT+DMFT.

B. Filling and ordering energy decomposition in DFT+U

Two important aspects of DFT+U calculations in correlated materials are (1) the total number of correlated (d or f) electrons per site and (2) the ordering of electrons within the correlated subspace based on spin (magnetism), angular momentum (orbital ordering), or site (CO). These two effects can be labeled as the "filling" and "ordering" of the correlated orbitals, respectively. Here we elucidate a decomposition of the interaction and dc energies that enables a useful decoupling of these two effects for analysis of DFT+U results. This spectral decomposition was also very briefly introduced in our previous work.[50]

To represent the average filling on a site we define the orbital occupancy mean

$$\mu_\tau = \frac{\sum_{m,s} n_m^{\tau s}}{N_{\text{orb}}}, \tag{6}$$

where $N_{\text{orb}} = \sum_{m,s} 1$ is the number of correlated spin-orbitals per site (e.g. 10 for the d shell). We then rewrite the interaction and dc energies to contain only terms containing the mean μ_τ or the deviation from the mean $n_m^{\tau s} - \mu_\tau$.

$$\begin{aligned}
E_U - E_{\text{dc}} &= \frac{1}{2}U \sum_{\tau,m,s} \left[n_m^{\tau s} - (n_m^{\tau s})^2\right] \\
&= \frac{1}{2}U \sum_{\tau,m,s} \left\{n_m^{\tau s} - \left[(n_m^{\tau s} - \mu_\tau)^2 - \mu_\tau^2 + 2n_m^{\tau s}\mu_\tau\right]\right\} \\
&= \frac{1}{2}U \sum_{\tau} \Bigg[\sum_{m,s} n_m^{\tau s} - \sum_{m,s} (n_m^{\tau s} - \mu_\tau)^2 + \\
&\qquad \mu_\tau^2 \sum_{m,s} 1 - 2\mu_\tau \sum_{m,s} n_m^{\tau s} \Bigg] \\
&= \frac{1}{2}UN_{\text{orb}} \sum_{\tau} \left[\mu_\tau - \mu_\tau^2 - \frac{\sum_{m,s}(n_m^{\tau s} - \mu_\tau)^2}{N_{\text{orb}}} \right] \\
&= \frac{1}{2}UN_{\text{orb}} \sum_{\tau} \left[\mu_\tau(1-\mu_\tau) - \sigma_\tau^2\right], \qquad (7)
\end{aligned}$$

where

$$\sigma_\tau = \sqrt{\frac{\sum_{m,s}(n_m^{\tau s} - \mu_\tau)^2}{N_{\text{orb}}}} \tag{8}$$

is the standard deviation of the occupancies for site τ. We call $\mu_\tau(1-\mu_\tau)$ the filling factor and σ_τ^2 the ordering factor, and at times in our discussion of results we drop the τ subscript on μ_τ and σ_τ for convenience. $E_U - E_{\text{dc}}$ is thus rewritten as $E_{\text{fill}} + E_{\text{ord}}$ with:

$$E_{\text{fill}} = \frac{1}{2}UN_{\text{orb}} \sum_{\tau} \mu_\tau(1-\mu_\tau) \tag{9}$$

and

$$E_{\text{ord}} = -\frac{1}{2}UN_{\text{orb}} \sum_{\tau} \sigma_\tau^2. \tag{10}$$

These terms encapsulate the two ways in which a system can avoid paying the Coulomb energetic penalty U. From the filling term, the system can minimize $\mu_\tau(1-\mu_\tau)$ by moving towards completely empty ($\mu_\tau = 0$) or completely filled ($\mu_\tau = 1$) correlated shells on average. From the ordering term, the system can maximize σ_τ^2 by enhancing the spread in $n_m^{\tau s}$ via some type of ordering. Note that $n_m^{\tau s}$ values for nominally-unoccupied orbitals still contribute to σ_τ, so this quantity is distinct from other measures of orbital ordering that are determined from low-energy orbitals (e.g. Wannier orbitals defined from a small energy window). One can rewrite E_U and E_{dc} in terms of μ_τ and σ_τ as

$$E_U = \frac{1}{2}UN_{\text{orb}} \sum_{\tau} \left[(N_{\text{orb}} - 1)\mu_\tau^2 - \sigma_\tau^2\right] \tag{11}$$

and

$$E_{\text{dc}} = \frac{1}{2}UN_{\text{orb}} \sum_{\tau} \mu_\tau(N_{\text{orb}}\mu_\tau - 1). \tag{12}$$

A function of only μ_τ, $-E_{\rm dc}$ takes the same form as $E_{\rm fill}$ except the prefactor on the quadratic term is $N_{\rm orb}$ instead of 1; E_U depends on both μ_τ and σ_τ.

In this work we are primarily interested in the formation energy, which is defined as

$$FE(x) = E(x) - [(1-x)E(0) + xE(1)], \qquad (13)$$

where $E(x)$ is the cohesive energy of a system with intercalant concentration x. The formation energy indicates whether a species of intermediate x has a higher or lower cohesive energy than the corresponding linear combination of those of the endmembers. Therefore, only energy terms beyond linear order in x contribute. The formation energy dictates the stability of such a species in the limit of low temperature ($T \to 0$); it is stable if negative and unstable if positive. One can separately construct the formation energy contributions stemming from $E_{\rm DFT}$, $E_U - E_{\rm dc}$, $E_{\rm fill}$, $E_{\rm ord}$ using expressions analogous expressions to Eq. 13, allowing one to understand the contribution of each term to the formation energy. Note that $FE_{\rm fill}$ will be negative if $\mu(1-\mu)$ is *lower* than the endmember linear combination, while $FE_{\rm ord}$ will be negative if σ^2 is *higher* than the endmember linear combination due to the negative sign in the definition of $E_{\rm ord}$ in Eq. 10. All formation energies reported in this work are normalized per formula unit (f.u.). We also compute the average intercalation voltage V via

$$eV = E({\rm Li}) + E(0) - E(1), \qquad (14)$$

where e is the elementary charge, E(Li) is the cohesive energy of body-centered-cubic Li, and the energies are normalized to the number of f.u.[51]

III. COMPUTATIONAL DETAILS

DFT+U calculations based on the spin-dependent generalized gradient approximation,[38] and the rotationally-invariant Hubbard U interaction[40] with J set to 0, and FLL dc are performed using the Vienna *ab initio* simulation package (VASP).[52–55] The projector augmented wave method[56,57] is employed and the single-particle equations are solved with a plane-wave basis set with a kinetic energy cutoff of 500 eV. We use a $9\times9\times9$ ($6\times7\times8$) k-point grid for the rhombohedral (orthorhombic) primitive unit cell of Li_xCoO_2 (Li_xFePO_4 and Li_xCoPO_4) and k-point grids with approximately the same k-point density for supercell calculations. The bulk lithium calculation is performed using a $19\times19\times19$ k-point grid. For structural relaxations in metals we employ the first-order Methfessel-Paxton method[58] with a 50 meV smearing and for all other calculations the tetrahedron method with Blöchl corrections[59] is used. The ionic forces, stress tensor components, and total energy are converged to 0.01 eV/Å, 10^{-3} GPa, and 10^{-6} eV, respectively.

The disordered (solid solution) phase of $Li_{1/2}CoO_2$ is modeled via the special quasirandom structure (SQS) approach[60] using the Alloy Theoretic Automated Toolkit (ATAT)[61,62] using point, pair, triplet, and quadruplet clusters. Candidate structures are generated based on the correlation functions of clusters with a maximum inter-site distance up to the in-plane 2nd nearest neighbor and out-of-plane 1st nearest neighbor distance. To evaluate the structures, we consider the minimal values of the following figure of merit: the root-sum-square of the differences between the cluster correlation functions and those of the random structure. In this evaluation, the correlation functions of clusters containing a maximum inter-site distance up to the in-plane 5th nearest neighbor and inter-plane 6th nearest neighbor are taken into account.

IV. RESULTS AND DISCUSSION

A. Endmember electronic structure within DFT

We begin by reviewing the electronic structure of the endmembers of Li_xCoO_2 and Li_xFePO_4 within DFT, comparing with the latest experimental understanding of these materials. $LiCoO_2$ crystallizes in the layered structure illustrated in Fig. 1(a) consisting of layers of edge-sharing CoO_6 octahedra and layers of Li. It has a rhombohedral primitive unit cell with the $R\bar{3}m$ space group and A-B-C (O3) oxygen stacking.[63,64] CoO_2 has a very similar structure with a hexagonal unit cell and A-B (O1) oxygen stacking in the $P\bar{3}m1$ space group.[65] Here for convenience we consider CoO_2 in the O3 structure, which has a very similar electronic structure to that of the O1 structure within DFT (see the Supplementary Material).

In Li_xCoO_2 the octahedral coordination of Co is slightly distorted due to the ability of the oxygens to relax in the out-of-plane direction, resulting in a symmetry lowering with $T_{2g} \to A_{1g} + E'_g$. Nominally $LiCoO_2$ is in the d^6 configuration with filled E'_g and A_{1g} levels, while CoO_2 has one fewer electron (d^5).

The p and d projection of the electronic density of states within DFT for CoO_2 and $LiCoO_2$ are shown in Fig. 2(a) and 2(b), respectively. $LiCoO_2$ is found to be a band insulator in agreement with experiments.[66–68] The computed band gap of 1.1 eV underestimates the experimental value of 2.7 eV as is typical for DFT.[66] The occupancies of A_{1g}, E'_g and E_g are 0.94, 0.95, and 0.41 for $LiCoO_2$, demonstrating that hybridization between Co d and O p states leads to appreciable occupation of the nominally-unoccupied E_g states. CoO_2 has a ferromagnetic low-spin metallic ground state with a Co magnetic moment of 0.8 μ_B. In experiments on CoO_2, there is evidence for Fermi liquid behavior and Pauli paramagnetism without any long-range magnetic ordering.[69–71] For CoO_2 the occupation of A_{1g}, E'_g and E_g are 0.96 (0.67), 0.96 (0.76), and 0.54 (0.52) for spin up (down) electrons, showing the significant degree of covalency in this system.

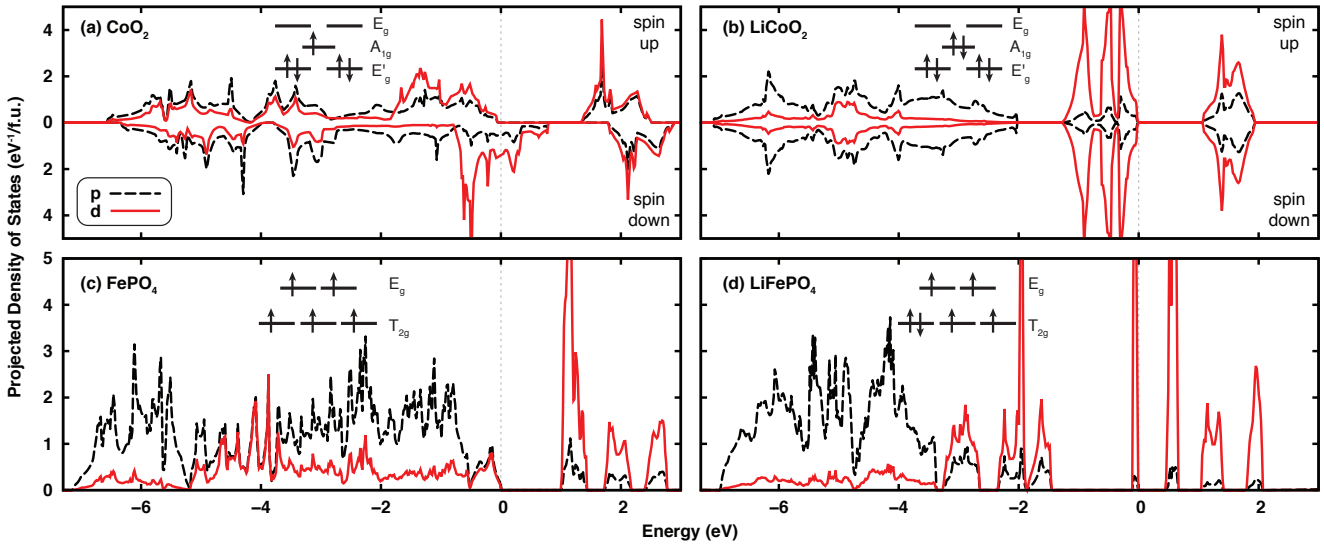

FIG. 2. Projected p and d density of states for (a) CoO_2, (b) $LiCoO_2$, (c), $FePO_4$, and (d) $LiFePO_4$ within DFT. For antiferromagnetic $FePO_4$ and $LiFePO_4$ only a single spin channel is shown. The dashed gray lines indicate the valence band maximum for insulators and the Fermi energy for metals. Insets are the nominal transition metal $3d$ orbital fillings from crystal field theory.

$LiFePO_4$ and $FePO_4$ both take on the olivine structure, which has an orthorhombic primitive unit cell containing 4 formula units in the *Pnma* space group.[72,73] The structure consists of corner-sharing FeO_6 octahedra layers connected via PO_4 tetrahedra as shown in Fig. 1(b). For $LiFePO_4$ there are one-dimensional chains of Li ions.

Li_xFePO_4 has significantly distorted FeO_6 octahedra, though for convenience we still crudely discuss the d orbitals as T_{2g} and E_g. Experimentally $LiFePO_4$ and $FePO_4$ are high-spin antiferromagnetic (AFM) insulators with Néel temperatures of 52 and 125 K, respectively.[72,73] While $FePO_4$ (d^5) nominally has all the d orbitals on a given site singly occupied with aligned spins (i.e., $S = 5/2$), for $LiFePO_4$ (d^6) there is one additional minority-spin electron in the T_{2g} manifold.[74,75] Fe linked via corner-sharing octahedra in the same layer have anti-aligned magnetic moments, while those laterally adjacent in different layers linked via PO_4 have aligned magnetic moments.[72,73]

The projected density of states for the olivine endmembers are shown in Fig. 2(c) and 2(d). Due to the antiferromagnetism, both spin channels are identical so only one is shown. $FePO_4$ can be viewed as a charge transfer type insulator since the gap is p–d in nature, whereas in $LiFePO_4$ d states form both the valence and conduction bands and the electronic bandwidths near the Fermi energy are extremely narrow (as little as 0.1 eV). Although $LiFePO_4$ has an even number of electrons, the local Coulomb interaction can play a strong role in developing or enhancing the insulating behavior. Within DFT, the band gaps of $FePO_4$ and $LiFePO_4$ are 1.0 eV and 0.4 eV, respectively. These values are brought much closer to agreement with the experimental band gaps of 1.9 eV[76] and 3.8 eV[76,77] using the DFT+U approach.[29,77]

B. Impact of U on electronic structure of Li_xCoO_2

The on-site interaction U has been computed as 4.9 and 5.4 eV for $LiCoO_2$ and CoO_2, respectively.[78] The U-dependence of the band gap and Co magnetic moment for Li_xCoO_2 are shown in Fig. 3. The band insulator $LiCoO_2$ has no magnetic moment and its band gap increases roughly linearly with U from 1.1 eV at $U = 0$ to 2.9 eV for $U = 5$ eV. Structural relaxations with U have little impact on the electronic structure. Note that we do not explore $U > 5$ eV since in this regime we find DFT+U predicts a high-spin state for $LiCoO_2$[26] in contradiction with experimental observation[67,68].

CoO_2 is semimetallic at lower values of U with the A_{1g} and E'_g states both partially occupied. Beyond $U = 1$ eV (or $U = 2$ eV when including structural relaxations), an orbital ordering occurs in which E'_g completely fills and A_{1g} becomes a nominally half-filled $S = 1/2$ state. This opens up a band gap of 0.5–1.2 eV and increases the Co magnetic moment to 1.1–1.4 μ_B, as compared to 0.7–0.8 μ_B for lower U.

The lowest-energy structure of $Li_{1/2}CoO_2$ has an in-plane ordering of Li and vacancies corresponding to the unit cell shown in Fig. 1(a) with the Li1 ion removed.[16–18] Experimental studies suggest $Li_{1/2}CoO_2$ is a paramagnetic metal with small Co magnetic moments of around 0.25–0.35 μ_B.[79–81] Within our calculations $Li_{1/2}CoO_2$ is a ferromagnetic metal for $U \leq 2$ eV

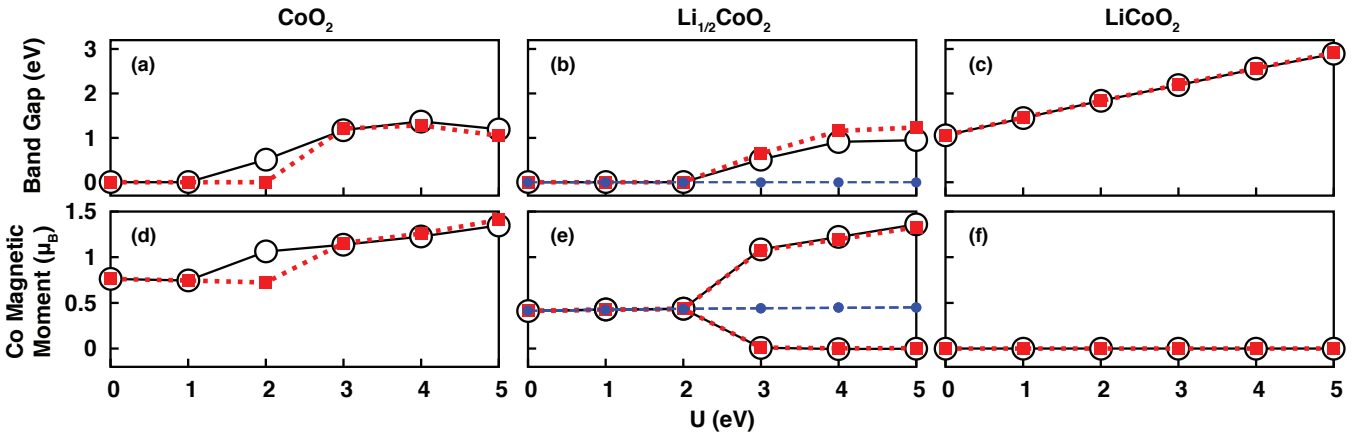

FIG. 3. Electronic band gap as a function of U for (a) CoO_2, (b) $Li_{1/2}CoO_2$, and (c) $LiCoO_2$ with relaxations (filled red squares) and with frozen $U = 0$ structures (large open black circles). The corresponding plots of Co magnetic moment are shown in panels (d)–(f). For panels (b) and (e), the additional small filled blue circles correspond to calculations with frozen $U = 0$ structures and CO suppressed.

with equal Co magnetic moments of 0.4 μ_B. For larger U values a new ground state with CO emerges in which the first site takes on a CoO_2-like configuration with a moment of 1.1–1.4 μ_B and the second takes on a $LiCoO_2$-like configuration with no moment (the actual charge difference between sites is small; see Fig. 4(a)). CO opens an electronic band gap that increases with U of 0.6–1.2 eV (0.5–0.9 eV without structural relaxations). Ignoring structural relaxations, the metallic state without CO is metastable and the Co magnetic moments are 0.4–0.5 μ_B and remain roughly constant for all values of U considered.

C. Tendency for charge ordering in DFT+U

To understand the tendency for CO in DFT+U, which is not observed in experiment, we investigated whether its origin is the interaction (U) term or the dc term. Given that the dc energy has a term which is a negative quadratic of N_d, it has a disposition towards charge ordering. Alternatively, the interaction term may indirectly drive CO as a means to reduce the interaction penalty, arising at the expense of E_{DFT}. To clearly identify the origin of CO, we implemented a modified DFT+U approach in which both the single-particle potential and total energy contributions stemming from the interaction term or the dc term are averaged over correlated sites. We call this site-averaged interaction and site-averaged dc, respectively.

Figure 4 illustrates the results of this computational experiment for ordered $Li_{1/2}CoO_2$ using the frozen $U = 0$ structure. With site-averaged dc (black squares) we still find a CO transition, for $U > 2$ eV. The magnitude of the CO in terms of N_d is slightly reduced, but the deviations in Co magnetic moment are the same or even more substantial than the standard DFT+U results (blue lines). The total energy shown in panel (c) for this case is only slightly (on the order of 10 meV/f.u.) higher than in the case of standard DFT+U, which indicates that the dc energetics are not very much lowered via CO. With site-averaged interaction (red circles), however, no CO can be obtained and the total energy is massively penalized as U increases (by hundreds of meV/f.u.). Therefore, we conclude that it is the interaction term and not the dc term that is responsible for the CO in DFT+U. This suggests that more accurate solutions to the interaction problem such as DMFT may be critical to resolving the issues associated with spurious CO.

D. Impact of U on phase stability of Li_xCoO_2

We first consider the formation energy of $Li_{1/2}CoO_2$ in the frozen $U = 0$ structure (i.e., no structural relaxations when imposing U) and without allowing CO, in order to purely see the effects of U in the absence of CO and lattice distortions. For the experimental Li ordering in $Li_{1/2}CoO_2$, the two Co atoms in the unit cell are equivalent by point symmetry. Therefore CO is a spontaneously broken symmetry, which enables one to precisely investigate various observables with and without CO. We will return to the effects of both CO and structural relaxations after thoroughly explaining the role of U in their absence.

As shown in Fig. 5(a), $Li_{1/2}CoO_2$ is phase stable with a total formation energy of -217 meV for $U = 0$. The formation energy increases monotonically with U and for $U > 3$ eV it becomes positive, corresponding to a prediction of phase separation. This indicates that the trend of a destabilization of compounds of intermediate x found previously in Li_xFePO_4[23] also occurs for Li_xCoO_2. Fur-

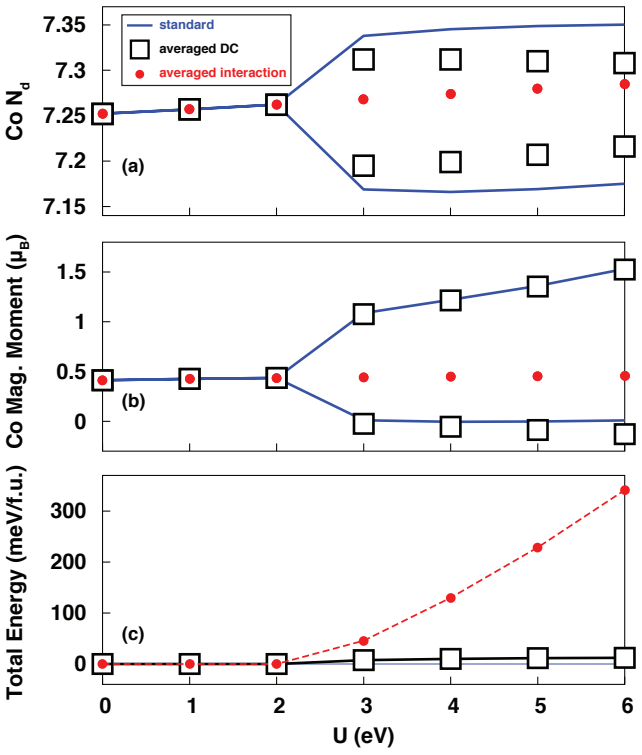

FIG. 4. (a) Co N_d, (b) Co magnetic moments, and (c) total energy for $Li_{1/2}CoO_2$ with the frozen $U = 0$ eV structure for standard DFT+U (blue lines) as well as with the interaction (filled red circles) or double counting (open black squares) terms averaged over correlated sites. Total energies in panel (c) are with respect to those of the standard DFT+U.

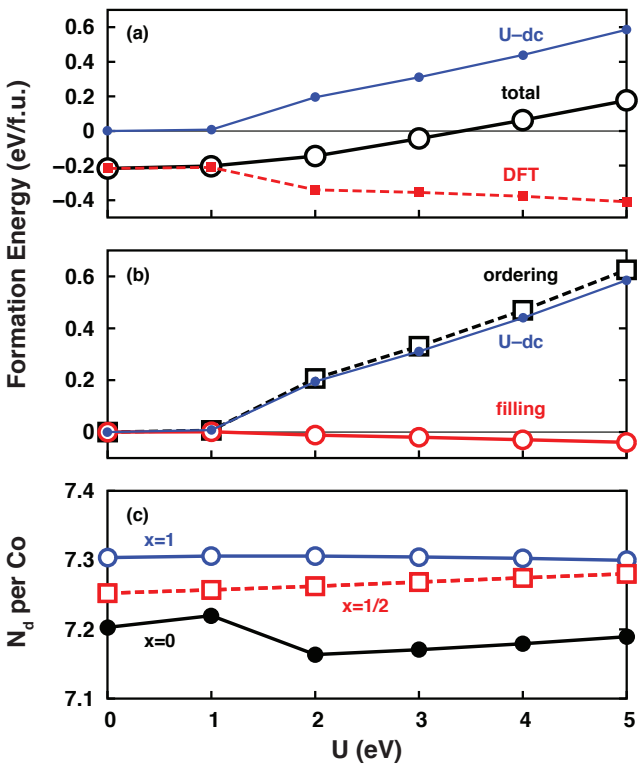

FIG. 5. (a) Total $Li_{1/2}CoO_2$ formation energy (open black circles) and its DFT (filled red squares) and U–dc (filled blue circles) components as a function of U (b) $Li_{1/2}CoO_2$ U–dc (filled blue circles) formation energy component and its orbital filling (open red circles) and orbital ordering (open black squares) components as a function of U (c) Number of d electrons per Co as a function of U for CoO_2 (filled black circles), $Li_{1/2}CoO_2$ (open red squares), and $LiCoO_2$ (open blue circles). All data correspond to the case of frozen $U = 0$ structures and CO suppressed in $Li_{1/2}CoO_2$.

thermore, it demonstrates that such a trend is found even in the absence of CO.

To illustrate the origin of this behavior, we also examine the DFT and U–dc components of the total formation energy in Fig. 5(a). For $U = 1$ eV the U–dc component is negligible (< 0.01 eV) and the slightly less negative value of formation energy (-203 meV) stems from the DFT component. Compared to the $U = 0$ values, for $U = 1$ eV the DFT energy increases by 17 meV for $Li_1/2CoO_2$ compared to only 7 meV for CoO_2 and 14 meV for $LiCoO_2$. For larger U the U–dc component is strongly positive and increases roughly linearly with U at a rate of around 130 meV per eV, leading to a more rapid increase in total formation energy. The DFT component has the opposite trend of becoming more negative with U, largely since the DFT energy of CoO_2 is strongly penalized by the orbital ordering, but the overall effect on the formation energy is smaller with changes of around 15–30 meV per eV. Therefore, it is the U–dc component that is responsible for the destabilization of $Li_{1/2}CoO_2$.

The number of d electrons per Co site (N_d) is plotted for $x = 0$, $x = 1/2$, and $x = 1$ as a function of U in Fig. 5(c). We note that the difference in N_d between CoO_2 and $LiCoO_2$ is only around 0.1 even though Li is nominally donating a full electron, which is due to the p–d rehybridization effect in Li_xCoO_2.[18,82] While the behavior of N_d is roughly constant at 7.3 for $LiCoO_2$ and smoothly increasing for $Li_{1/2}CoO_2$ between 7.25 and 7.28, there is discontinuous behavior for CoO_2 in which N_d drops from 7.22 to 7.16 from $U = 1$ to $U = 2$ eV corresponding to the orbital ordering. This change in electronic structure in the $x = 0$ endmember is responsible for the change in behavior in the U–dc formation energy contribution.

Since the dc term in Eq. 4 is a negative quadratic function, one might expect that the dc is responsible for the trend towards phase separation. This simple line of reasoning immediately becomes more complicated given that N_d is a nonlinear function of x as demonstrated in Fig. 5(c), and a careful analysis in Sec. IV H shows that it is not the dc that drives phase separation. Alternatively, we proceed to understand the contributions of both the E_U and E_{dc} terms simultaneously in a different framework using the energy decomposition described in Sec. II B. In Fig. 5(b) we break down the U–dc for-

mation energy contribution into the filling and ordering contributions. Remarkably, the magnitude of the filling contribution contributes negligibly, only being at most tens of meV in magnitude, whereas essentially all of the U–dc formation energy comes from the ordering term. Therefore, it is the ordering rather than the filling of the correlated d orbitals that drives phase separation.

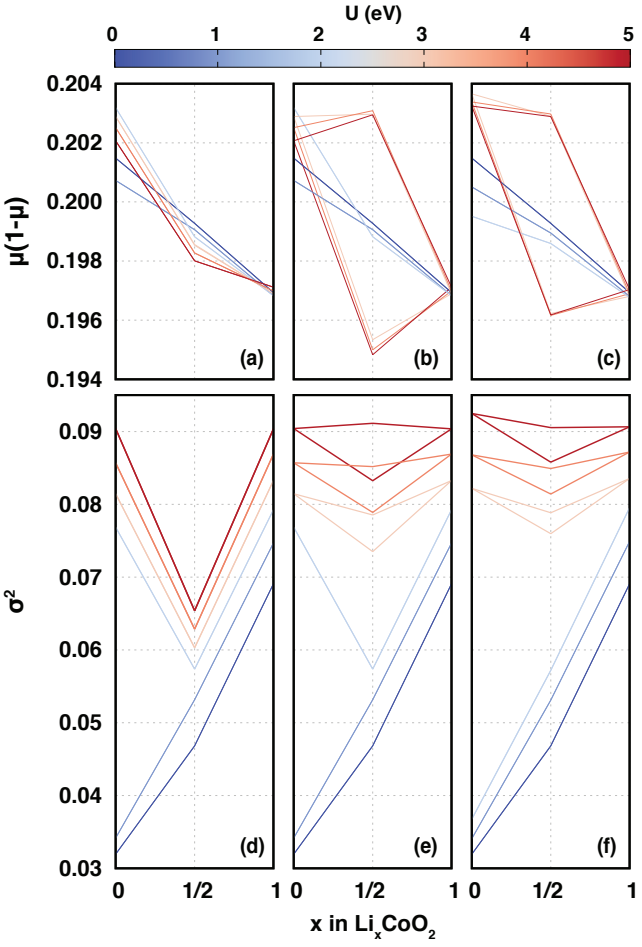

FIG. 6. Filling factor $\mu(1-\mu)$ as a function of x for different U in Li_xCoO_2 for (a) frozen $U = 0$ structures and CO suppressed, (b) frozen $U = 0$ structures and CO allowed, and (c) relaxed structures. Panels (d)–(f) show the corresponding plots for the ordering factor σ^2. The two lines per U in some plots correspond to the two distinct Co sites in $Li_{1/2}CoO_2$. The line thickness increases for increasing values of U.

The individual filling factor $\mu(1-\mu)$ and ordering factor σ^2 as a function of Li concentration for different U are shown for this case in Fig. 6(a) and 6(d), respectively. We note that based on nominal electron counting $\mu(1-\mu)$ will be 0.25 for Co^{4+} and 0.24 for Co^{3+}. Consistent with this expectation, we observe that the filling factor is highest for $x = 0$ and lowest for $x = 1$. The actual values for Li_xCoO_2 are lower in magnitude (around 0.2) due to the substantial covalent nature of the bonding, in particular the hybridization of O p states with Co E_g states. Although this filling factor magnitude is around half an order of magnitude higher than that of the ordering factor, the relative deviations of the $x = 1/2$ value compared to the average of the $x = 0$ and $x = 1$ values are tiny (around 10^{-3} electrons). This is why filling term leads to a negligible contribution to the formation energy.

The values of σ^2 increase with U for all x in agreement with the expectation that the U and dc parts of the total energy functional will penalize fractional orbital occupancy (i.e., $0 < n_m^{\tau s} < 1$). For $U \leq 1$ eV σ^2 is nearly linear in x, thus leading to no appreciable formation energy contribution. However, once CoO_2 undergoes the orbital ordering, its value of σ^2 significantly increases from 0.03 to 0.08. After this phase transition, σ for $Li_{1/2}CoO_2$ is substantially lower than the average of those of CoO_2 and $LiCoO_2$. For example, for $U = 2$ eV σ is 0.277 for CoO_2 and 0.282 for $LiCoO_2$ but only 0.239 for $Li_{1/2}CoO_2$. This lower-than-average σ^2 is translated to a positive formation energy contribution via the negative sign in prefactor of Eq. 10.

The fundamental behavior we find is that U drives phase separation via enhanced ordering of the correlated orbitals for the endmembers relative to the species with intermediate Li concentration. Given that we restricted the possibility of CO, $Li_{1/2}CoO_2$ has no low energy means to orbitally order and keep pace with CoO_2 as U is increased. We will articulate this important point in a bit more detail. For $U \leq 1$ eV σ^2 is much smaller for $x = 0$ than $x = 1$; CoO_2 has a smaller range of $n_m^{\tau s}$ due to its semimetallic behavior and enhanced hybridization with O p states. Once it has orbitally ordered at $U = 2$ eV and the hole in the T_{2g} manifold is localized in the minority-spin A_{1g} state, however, CoO_2 has 5 very occupied d orbitals ($n_m^{\tau s} \geq 0.96$) and 5 much less occupied orbitals ($n_m^{\tau s}$ of around 0.15 for minority-spin A_{1g} and higher values of 0.49–0.59 for E_g due to p–d hybridization). $LiCoO_2$ is a band insulator, so there is no abrupt change in σ^2 as a function of U. In terms of σ^2, $LiCoO_2$ behaves very similarly to CoO_2 in the regime of U in which CoO_2 is orbitally ordered. In $LiCoO_2$ there are 6 very occupied d orbitals ($n_m^{\tau s} \approx 0.96$ for A_{1g} and E_g' states) and 4 much less occupied orbitals ($n_m^{\tau s} = 0.39$ for E_g states). This gives a large spread (σ) in orbital occupancies for $LiCoO_2$ in addition to CoO_2. In contrast, for $Li_{1/2}CoO_2$ we have a metallic state with a nominally half-filled minority-spin A_{1g} level ($n_m^{\tau s} \approx 0.61$) and thus smaller σ^2. This lower-than-average σ^2 for $Li_{1/2}CoO_2$ is what results in a positive contribution to the formation energy from the U–dc energetics.

This same type of behavior is preserved even when we now allow CO in $Li_{1/2}CoO_2$, though CO will allow $Li_{1/2}CoO_2$ to order and completely avoid phase separation for all U (we still restrict the possibility of structural relaxations until later in this analysis). Fig. 7 shows the results with the frozen $U = 0$ structures but now allowing for CO in $Li_{1/2}CoO_2$. Here again the formation energy increases with U. For small values of U the increase is

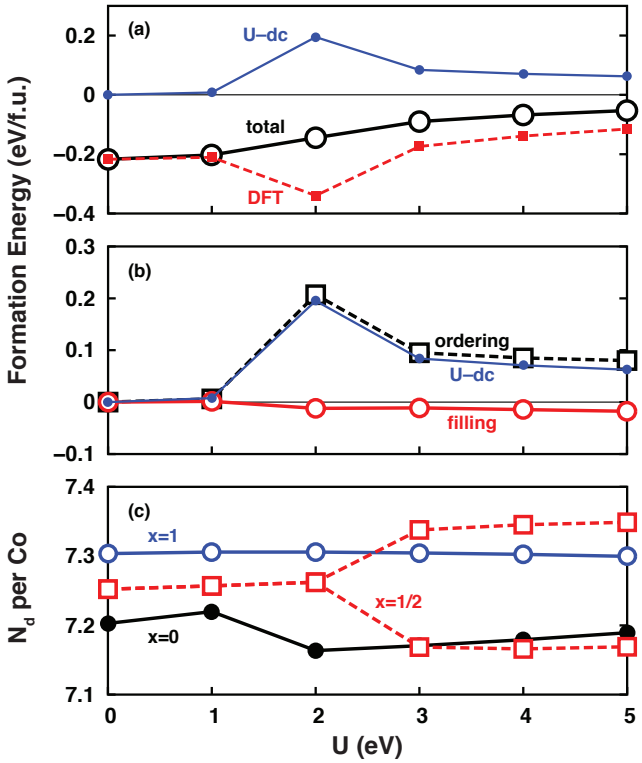

FIG. 7. (a) Total $Li_{1/2}CoO_2$ formation energy (open black circles) and its DFT (filled red squares) and U–dc (filled blue circles) components as a function of U (b) $Li_{1/2}CoO_2$ U–dc (filled blue circles) formation energy component and its orbital filling (open red circles) and orbital ordering (open black squares) components as a function of U (c) Number of d electrons per Co as a function of U for CoO_2 (filled black circles), $Li_{1/2}CoO_2$ (open red squares), and $LiCoO_2$ (open blue circles). All data correspond to the case of frozen $U = 0$ structures and CO allowed and the two lines in panel (c) for $Li_{1/2}CoO_2$ correspond to the two distinct Co sites.

small and stems from the DFT contribution. After CoO_2 orbitally orders and opens a band gap, the U–dc energetics are a phase separating contribution to the total formation energy. As before, essentially all of the U–dc contribution comes from the ordering, not the filling, of the d orbitals. When $Li_{1/2}CoO_2$ charge orders for U greater than 2 eV, the U–dc phase separating contribution is significantly dampened but there is always still a positive phase separating contribution (53–84 meV). CO also leads to an increase in the DFT formation energy contribution from -0.34 eV at $U = 2$ eV to -0.17 eV at $U = 3$ eV.

As illustrated in Fig. 6(b) and 6(e), the variations in filling factor $\mu(1-\mu)$ are again negligible so the only appreciable component to the U–dc energetics stems from the changes in ordering factor σ^2. The CO of $Li_{1/2}CoO_2$ significantly increases the average σ^2, but it still always lags behind the average of those of CoO_2 and $LiCoO_2$. For example, for $U = 5$ eV $E_{\rm ord}$ is 87 meV for $x = 1/2$ and 90 meV for the average for the $x = 0$ and $x = 1$ values. In this case we still end up with a total formation energy that steadily increases with U, though now CO dampens the process substantially such that for $U = 5$ eV the value remains negative consistent with experiment.

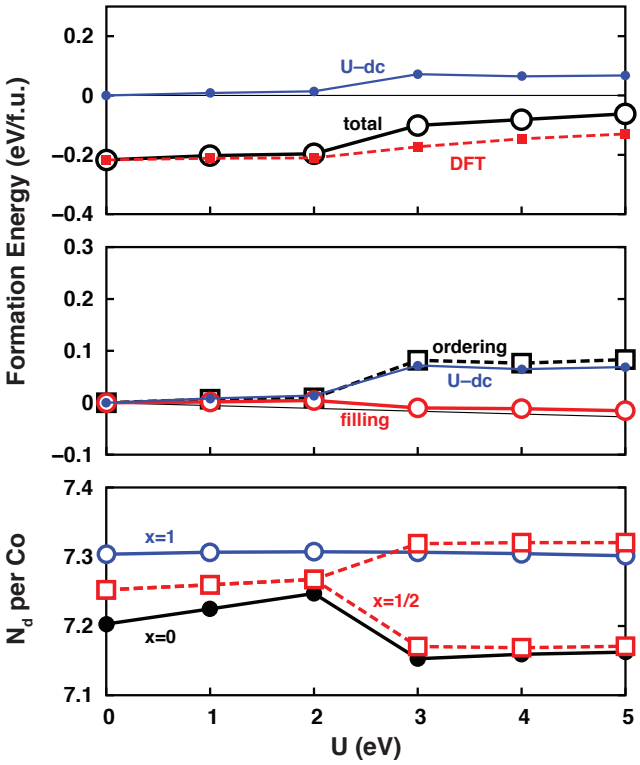

FIG. 8. (a) Total $Li_{1/2}CoO_2$ formation energy (open black circles) and its DFT (filled red squares) and U–dc (filled blue circles) components as a function of U (b) $Li_{1/2}CoO_2$ U–dc (filled blue circles) formation energy component and its orbital filling (open red circles) and orbital ordering (open black squares) components as a function of U (c) Number of d electrons per Co as a function of U for CoO_2 (filled black circles), $Li_{1/2}CoO_2$ (open red squares), and $LiCoO_2$ (open blue circles). All data correspond to the case of fully relaxed structures and the two lines in panel (c) for $Li_{1/2}CoO_2$ correspond to the two distinct Co sites.

When we include CO in $Li_{1/2}CoO_2$ and full structural relaxations, we find the same fundamental effect as in the previous case only allowing CO: structural relaxations only provide a further dampening. As shown in Fig. 8, the total formation energy increases with U and the positive contribution stems from the ordering component of the U–dc energetics. Here the CO and CoO_2 orbital ordering both occur for $U > 2$ eV. The increase in the DFT formation energy contribution upon CO is dampened due to relaxations. The total formation energy remains negative at -61 meV at $U = 5$ eV. The plots of $\mu(1-\mu)$ and σ^2 are shown in Fig. 6(c) and 6(f), respectively. Structural relaxations serve to slightly enhance σ^2 for CoO_2 and decrease the difference in σ^2 for the distinct Co sites

in $Li_{1/2}CoO_2$.

These results have significant implications on the accuracy and robustness of the DFT+U description of strongly correlated materials. Without CO, which is not found in experiments on this class of materials, DFT+U incorrectly predicts that Li_xCoO_2 phase separates once U becomes appreciable. This is true even if we allow structural relaxations while suppressing CO, which is possible since CO is a spontaneously broken symmetry in $Li_{1/2}CoO_2$, and in this case the total formation energy values are -40 meV, +67 meV, and +182 meV for U of 3, 4, and 5 eV, respectively. That DFT+U requires artificial CO to correctly capture the phase stable nature of Li_xCoO_2 is a significant weakness of this approach.

E. Impact of U on electronic structure of Li_xFePO_4

The interaction U has been computed as 3.7 and 4.9 eV for $LiFePO_4$ and $FePO_4$, respectively.[78] The variation of the band gap, total magnetization, and Fe magnetic moment as a function of U for Li_xFePO_4 is illustrated in Fig. 9. The endmembers are both AFM so there is zero net magnetization. The Fe magnetic moment, which increases approximately linearly with U, is 4.0–4.4 μ_B for $FePO_4$ and 3.6–3.8 μ_B for $LiFePO_4$ for 0 eV $\leq U \leq$ 6 eV. The endmembers are both insulating. For this U range the band gaps increases from 1.0 to 2.7 eV for $FePO_4$ and 0.4 to 4.5 eV, a much larger range, for $LiFePO_4$. Very similar results for the endmembers are found when one freezes the ions to the experimental structures.

For intermediate x we consider the lowest-energy configurations that fit within the primitive unit cell shown in Fig. 1(b). The structures correspond to removing Li2, Li3, and Li4 for $x = 1/4$, Li3 and Li4 for $x = 1/2$, and Li4 for $x = 3/4$.[23] Calculations on the two other possible primitive cell $Li_{1/2}FePO_4$ structures are always found to be higher in energy, so we do not discuss them here. In addition to the case in which structures are fully relaxed, we also perform calculations on structures constructed via linear interpolation of the experimental $x = 0$ and $x = 1$ structures. This is an ideal manner to isolate the effect of lattice relaxations given that appreciable lattice distortions arise in the intermediate compounds even for $U = 0$.

For $U = 0$ the intermediate x species of Li_xFePO_4 are AFM metals without any CO. The Fe magnetic moments are 3.9, 3.8, and 3.7 μ_B for $x = 1/4$, $x = 1/2$, and $x = 3/4$, respectively. The magnetic moment magnitude gradually increases with U, and above critical U values a CO transition occurs leading to distinct Fe^{3+}-like (d^5) and Fe^{2+}-like (d^6) sites within the primitive unit cell. This symmetry breaking leads to distinct local magnetic moments and the opening of an electronic band gap. Unlike Li_xCoO_2 for which N_d differences among correlated sites are 0.15-0.18 electrons in the CO state, Li_xFePO_4 has CO states with substantially larger N_d differences around 0.4 electrons due to the highly localized nature of this system.

For $Li_{1/2}FePO_4$ using the frozen structure (linear interpolation of endmember experimental structures), the CO transition at $U > 4$ eV yields a ferrimagnetic state with total magnetization 2 μ_B; there are 2 Fe magnetic moments of 3.7 μ_B (Fe^{2+}-like) and 2 Fe magnetic moments of -4.3 μ_B (Fe^{3+}-like). It opens a band gap of 0.6 eV for $U = 4.7$ eV that is further increased with U to a value of 1.1 eV for $U = 5.9$ eV. Including structural relaxations has little effect on the electronic structure in the regime of U before the onset of CO. However, relaxations assist the CO transition and result in a lower critical value of $U = 2$ eV above which the CO state remains AFM with Fe magnetic moments of $\pm$ 3.7 and $\pm$ 4.2 μ_B. In addition, relaxation serves to enhance the band gap of the CO state to values of 0.4–2.2 eV.

$Li_{1/4}FePO_4$ and $Li_{3/4}FePO_4$ show similar behavior in which at critical values of U (lower when structural relaxation is included) a CO transition opens an electronic band gap. For $Li_{1/4}FePO_4$ with (without) relaxations a band gap opens at $U = 4$ eV (5.3 eV) when CO yields 1 Fe^{3+}-like site and 3 Fe^{2+}-like sites. For $Li_{3/4}FePO_4$ with (without) relaxations a band gap opens at $U = 3$ eV (5.3 eV) when CO yields 3 Fe^{3+}-like sites and 1 Fe^{2+}-like site. For $x = 1/4$ and $x = 3/4$ the magnitude of the band gap is around 0.1–0.6 eV for the frozen structures and a larger values of 0.5–1.8 eV including relaxations. For these x, the CO transition always leads to a ferrimagnetic state with magnetization of 1 μ_B. The Fe magnetic moments of the distinct sites are around 3.8 and 4.4 μ_B and slowly increase with U as in the case of $x = 1/2$. Differences in the magnetic moments between the frozen and relaxed structures in the CO regime are small. We note that for these x, unlike in $x = 1/2$, we find partial CO for intermediate values of U in which the Fe magnetic moments begin to take on slightly different values without the presence of a band gap. For example, including relaxations for $U = 1$ eV $Li_{1/4}FePO_4$ is metallic with Fe magnetic moments of 3.9, -3.9, -4.0, and 4.0 μ_B. This indicates DFT+U is driving Li_xFePO_4 towards CO even for small U, which is to be expected given the very narrow bandwidths.

Unlike for Li_xCoO_2 (see Fig. 3), for Li_xFePO_4 the CO is stabilized by structural relaxations as evidenced by the lower critical U values for CO. The stabilization of CO by structural relaxations suggests stronger coupling between the electronic and lattice degrees of freedom in Li_xFePO_4 as compared to Li_xCoO_2. This is consistent with the evidence for polarons in Li_xFePO_4.[76,83]

F. Impact of U on phase stability of Li_xFePO_4

The formation energy behavior for Li_xFePO_4 as a function of U without allowing for the effect of structural relaxations is summarized in Fig. 10. The behavior shares many similarities and a few differences to that of Li_xCoO_2, which we will describe. As illustrated in panels

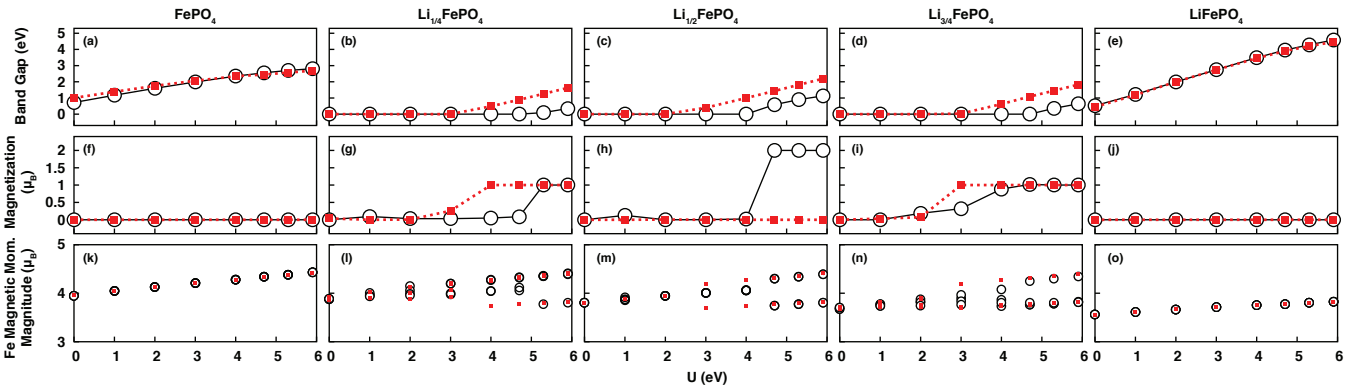

FIG. 9. Electronic band gap as a function of U for (a) $FePO_4$, (b) $Li_{1/4}FePO_4$, (c) $Li_{1/2}FePO_4$, (d) $Li_{3/4}FePO_4$, and (e) $LiFePO_4$ with relaxations (filled red squares) and with frozen linearly interpolated experimental structures (open black circles). The corresponding plots of total magnetization and Fe magnetic moment magnitudes are shown in panels (f)–(j) and (k)–(o), respectively. For panels (k)–(o), the multiple symbols per U correspond to the 4 distinct Fe sites.

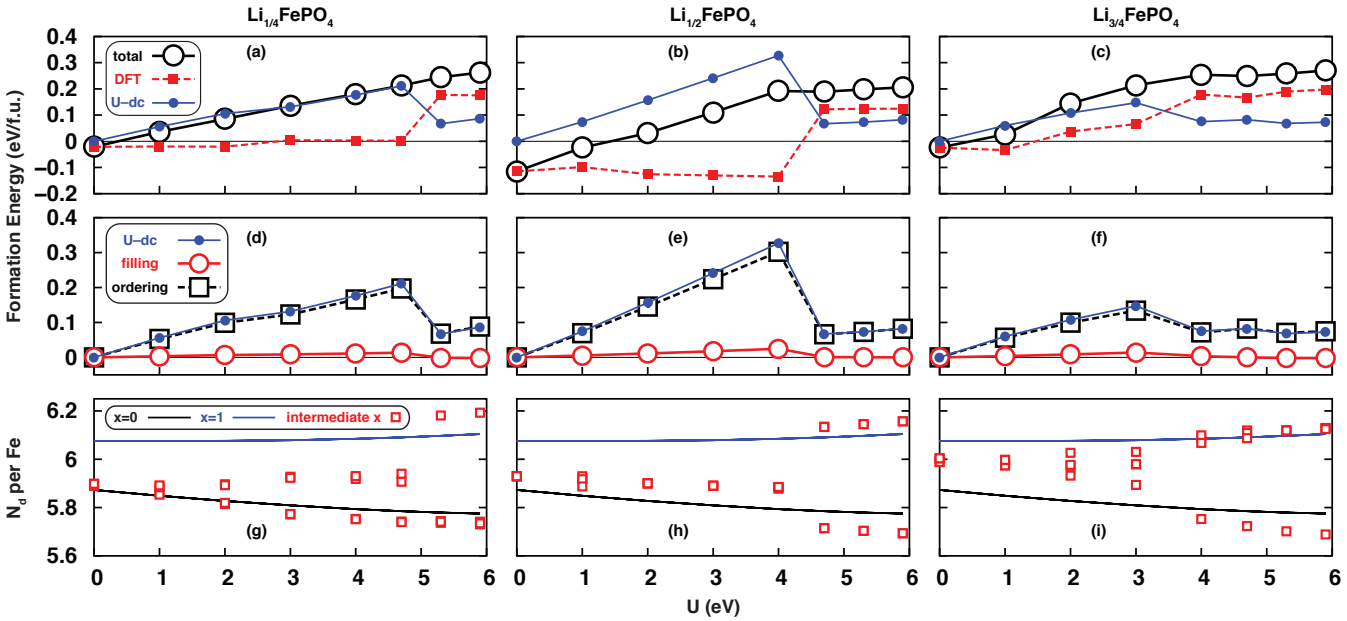

FIG. 10. Total Li_xFePO_4 formation energy (open black circles) and its DFT (filled red squares) and U–dc (filled blue circles) components as a function of U for (a) $x = 1/4$, (b), 1/2, and (c) $x = 3/4$. (d)–(f) show the corresponding plots of Li_xFePO_4 U–dc (filled blue circles) formation energy component and its orbital filling (open red circles) and orbital ordering (open black squares) components as a function of U. (g)–(i) show the corresponding plots of number of d electrons per Fe as a function of U for $FePO_4$ (black line), Li_xFePO_4 (open red squares), and $LiFePO_4$ (blue line). All data correspond to the case of frozen linearly interpolated experimental structures.

(a)–(c), for all intermediate x the total formation energy increases with U as in the case of Li_xCoO_2 and changes sign from negative to positive for sufficiently high U. For example, for $x = 1/2$ the formation energy is -0.11 eV at $U = 0$ and increases to $+0.21$ eV for $U = 5.9$ eV. For $x = 1/4$ and $x = 3/4$, there are only slightly negative values of around -0.02 eV for $U = 0$, which increase to as much as $+0.26$–0.27 eV as U increases. We note that the formation energies are higher for this frozen structure case since the intermediate x species will exhibit more significant structural relaxations than the endmembers.

For most of the U range, that below the critical U for CO, the DFT component of the formation energy is approximately constant and does not strongly influence phase stability. For example, for $x = 1/4$ this component varies by only 25 meV for 0 eV $\leq U \leq$ 4.7 eV. In contrast, the U–dc component of the formation energy undergoes significant changes as it increases roughly lin-

early with U; the change is 0.21 eV over the same U range for $x = 1/4$. This U–dc contribution is positive and therefore, as in the case of Li_xCoO_2, is what drives the total formation energy towards phase separation in Li_xFePO_4 in this regime before CO. One caveat to this characterization is that the DFT component varies more considerably (by 90 meV) for $Li_{3/4}FePO_4$ in this regime. In this case it is positive for 2 eV $\leq U \leq$ 3 eV and thus can be described as partially responsible for the positive total formation energy.

Upon CO there is a drastic change in the formation energy components, as in the case of Li_xCoO_2. The U–dc component drops steeply to much smaller values of around 0.06–0.08 eV. For $x = 1/2$, for example, the value is 0.33 eV for $U = 4$ eV and only 0.07 eV for $U = 4.7$ eV due to the CO transition; the drop in the U–dc contribution is substantial though smaller in magnitude for $x = 1/4$ and $x = 3/4$. Here as in Li_xCoO_2 we also find an increase in the DFT formation energy contribution due to CO. For example, for $Li_{1/2}FePO_4$ the DFT formation energy contribution jumps from -135 meV to $+122$ meV across the CO phase boundary. Unlike in $Li_{1/2}CoO_2$ [see Fig. 7(a)], for $Li_{1/2}FePO_4$ the increase in the DFT component is enough to make it positive. It is even larger in magnitude than the U–dc component. For $x = 1/4$ and $x = 3/4$ the DFT component is already positive but it becomes substantially more positive after CO. Despite how sharp the changes in formation energy components are, the total formation energy changes less abruptly from CO. For example, for $x = 1/2$ the total formation energy changes only by 3 meV between $U = 4$ eV and $U = 4.7$ eV. After the CO transition, the formation energy and its components are relatively flat versus U. For $x = 1/2$, for example, the changes are on the order of only 15–25 meV.

The breakdown of U–dc formation energy into filling and ordering contributions is shown in Fig. 10(d)–(f). As in Li_xCoO_2, it can be seen that the average filling contributes negligibly to the phase separation; the maximum contribution is at most 25 meV and typically much smaller. Therefore, again the impact of U and the dc is essentially entirely contained within the ordering contribution. The ordering contribution tracks the behavior of the total U–dc term and it can be as much as +0.3 eV.

The plots of N_d on each Fe site versus U in Fig. 10(g)–(i) illustrate that there is also a p–d rehybridization mechanism in Li_xFePO_4 similar but smaller than that in Li_xCoO_2 with differences in N_d around 20–30% of a full electron between $x = 0$ and $x = 1$. Like the Fe magnetic moment data in Fig. 9, these N_d values illustrate the partial and full CO that occurs as U increases. We note that without structural relaxations the spread in N_d values after CO for the intermediate x can be larger than the difference between N_d of $x = 0$ and $x = 1$. We find the behavior of N_d with x is complex and system dependent: in this case N_d for intermediate x is generally lower than the endmember linear interpolation, whereas in Li_xCoO_2 the opposite is true.

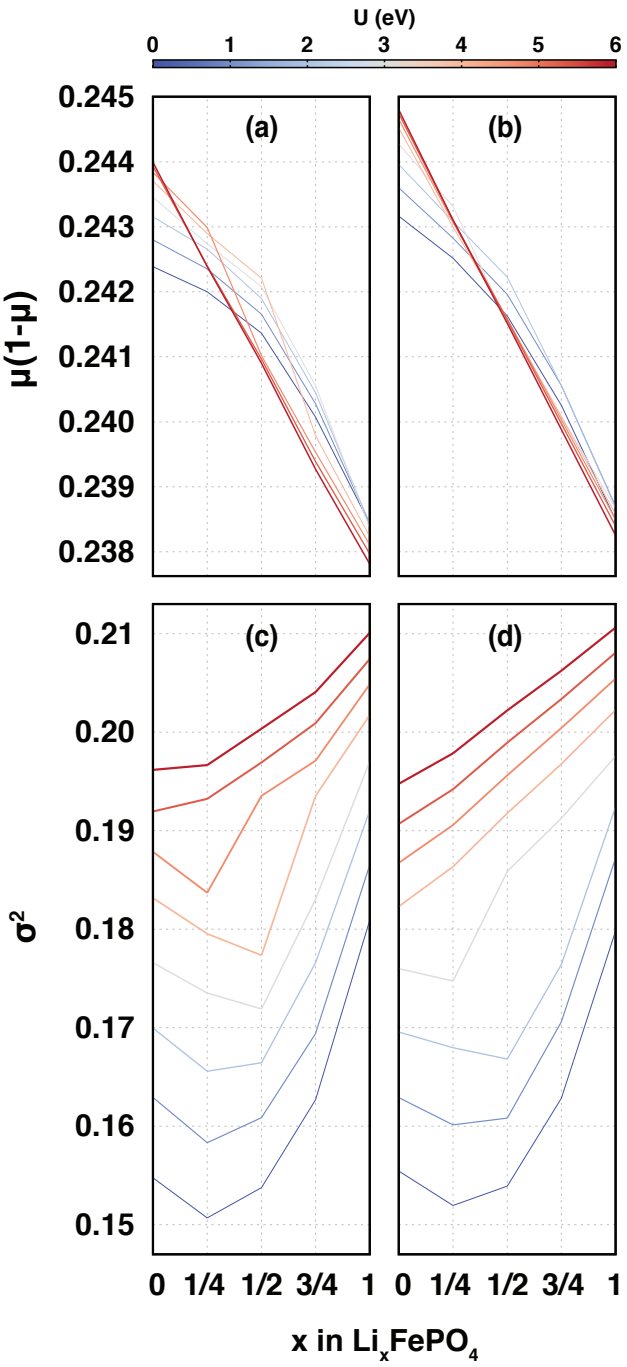

FIG. 11. Filling factor $\mu(1-\mu)$ as a function of x averaged over Fe sites for different U in Li_xFePO_4 for (a) linearly interpolated experimental structures and (b) relaxed structures. Panels (c) and (d) show the corresponding plots for the ordering factor σ^2. The line thickness increases for increasing values of U.

To investigate the origin of the positive U–dc phase-separating contribution to the total formation energy for Li_xFePO_4, in Fig. 11 we plot the individual $\mu(1-\mu)$ [panel (a)] and σ^2 [panel (c)] values as a function of x for different U. For clarity, we take the average over the 4 Fe sites in the primitive unit cell. As in the case of Li_xCoO_2, the magnitude of the filling factor is high (around 0.24) but the changes with respect to the average of the endmember values are very small (on the order of 10^{-3}). This is responsible for the negligible contribution of the filling component to the total formation energy. As for Li_xCoO_2, the filling factor is highest for $x = 0$ and $x = 1$. Compared to those of Li_xCoO_2, the $\mu(1-\mu)$ values of Li_xFePO_4 are much nearer to the range expected from nominal electron counting for Fe^{2+} and Fe^{3+} (0.24–0.25) since there is less hybridization between p and d states. This is also the reason for the enhanced magnitude of σ^2 compared to that of Li_xCoO_2.

Compared to $\mu(1-\mu)$, σ^2 has a smaller but still significant magnitude (around 0.18) for Li_xFePO_4. The σ^2 values monotonically increase with U (by around 0.003–0.006 per eV) for all x, which as in the case of Li_xCoO_2 is expected since the U and dc terms serve to enhance orbital polarization in the correlated subspace. Unlike in $\mu(1-\mu)$, there are substantial deviations of the σ^2 values for intermediate x compared to the endmember average. For example, for $x = 1/2$ at $U = 3$ eV σ^2=0.172 as compared to 0.187 for the endmember average. The ordering factor is consistently lower than the endmember linear interpolation, thus leading to the positive formation energy contribution.

One can observe a moderate increase in σ^2 values for intermediate x upon CO. For example, for $x = 1/2$ σ^2 jumps from 0.177 to 0.194 upon CO at $U = 4.7$ eV. However, as in the case of Li_xCoO_2 the σ^2 values still are always lower than the linear interpolation of $x = 0$ and $x = 1$ values even after CO. For example, the endmember average σ^2 is 0.196 for $U = 4.7$ eV so it is still slightly larger than the value for $Li_{1/2}FePO_4$. Therefore, we find that CO alleviates but does not eliminate the tendency for phase separation with U derived from the ordering of correlated orbitals.

Figure 12(a)–(c) shows the formation energy behavior of Li_xFePO_4 including full structural relaxations. In this case, since there are more significant total energy lowerings from relaxing the intermediate x structures compared to those from relaxing the endmembers, the total formation energy values are significantly lower. For example, for $Li_{1/4}FePO_4$ the maximum formation energy is 52 meV as opposed to 262 meV in the case of linearly interpolated endmember experimental structures. Otherwise, the behavior is generally similar to the case without relaxations. For all x, the total formation energy increases monotonically with U and for sufficiently high U switches from negative to positive. We note that the formation energy $Li_{1/2}FePO_4$ is only slightly positive (+6.7 meV) for the largest U we considered. This is in quantitative disagreement with the original DFT+U work[23] for reasons which are not clear, but is consistent with a more recent report.[24]

Here again the DFT formation energy contribution is approximately constant (deviations of at most 25 meV and typically less) before the CO transition with a slight tendency to increase with U. In this case $x = 3/4$ is no longer an exception to the general trend. In contrast, the U–dc contribution is positive and significantly increases (roughly linearly) with U. The largest value it takes on is 151 meV for $x = 1/2$ at $U = 2$ eV. Therefore, again it is the positive U–dc contribution that destabilizes the compounds of intermediate x in this regime.

After CO, the U–dc formation energy contribution is significantly dampened but remains positive. For example, for $x = 1/4$ it decreases from 106 to 18 meV at the CO phase boundary. The effect is similarly substantial for all x. At the same time, the DFT formation energy component abruptly increases due to CO and becomes positive ($x = 1/4$ and $x = 3/4$) or much less negative ($x = 1/2$). The magnitude of this increase is more substantial than that of Li_xCoO_2, which suggests that in Li_xFePO_4 CO constitutes a more significant rearrangement of charge density. The net effect is that upon CO the increase in total formation energy with U is slowed. For the $x = 1/4$ case, for example, the total formation energy increases only by 12 meV from $U = 3$ to $U = 4$ eV as opposed to the lower-U regime in which the same change in U yields increases of around 46 meV. In the CO state both the DFT and U–dc components of the formation energy are nearly constant with respect to U. As such, the total formation energies saturate to around +50, +6, and +50 meV for $x = 1/4$, $x = 1/2$, and $x = 3/4$ in the regime of large U.

As illustrated in Fig. 12(d)–(f), in this case again the positive U–dc formation energy contribution stems entirely from the ordering contribution (from the spread in orbital occupancies); the filling component (from the average orbital occupancy) is negligible with values less than 10 meV. CO lowers the filling contribution even further to no more than 1 meV. In contrast, the ordering contribution is dampened but still positive and appreciable; it tracks the behavior of the total U–dc formation energy contribution.

The evolution of the N_d values into two discrete groups (Fe^{3+}- and Fe^{2+}-like) due to CO is shown in Fig. 12(g)–(i). A similar magnitude of p-d rehybridization is observed based on the overall range of N_d. As in the case without structural relaxations, here for $x = 1/4$ and $x = 3/4$ though not $x = 1/2$ there is a regime of intermediate x in which there is partial CO in metallic states. After the CO transition the two groups of N_d values closely match those of $x = 0$ and $x = 1$, which suggests the CO is very complete and the local environments of Fe for intermediate x mimic those of the endmembers.

The filling and ordering factors for relaxed Li_xFePO_4 are shown in Fig. 11(b) and 11(d), respectively. We find similar results when including structural relaxations. The deviations in $\mu(1-\mu)$ with respect to the linear in-

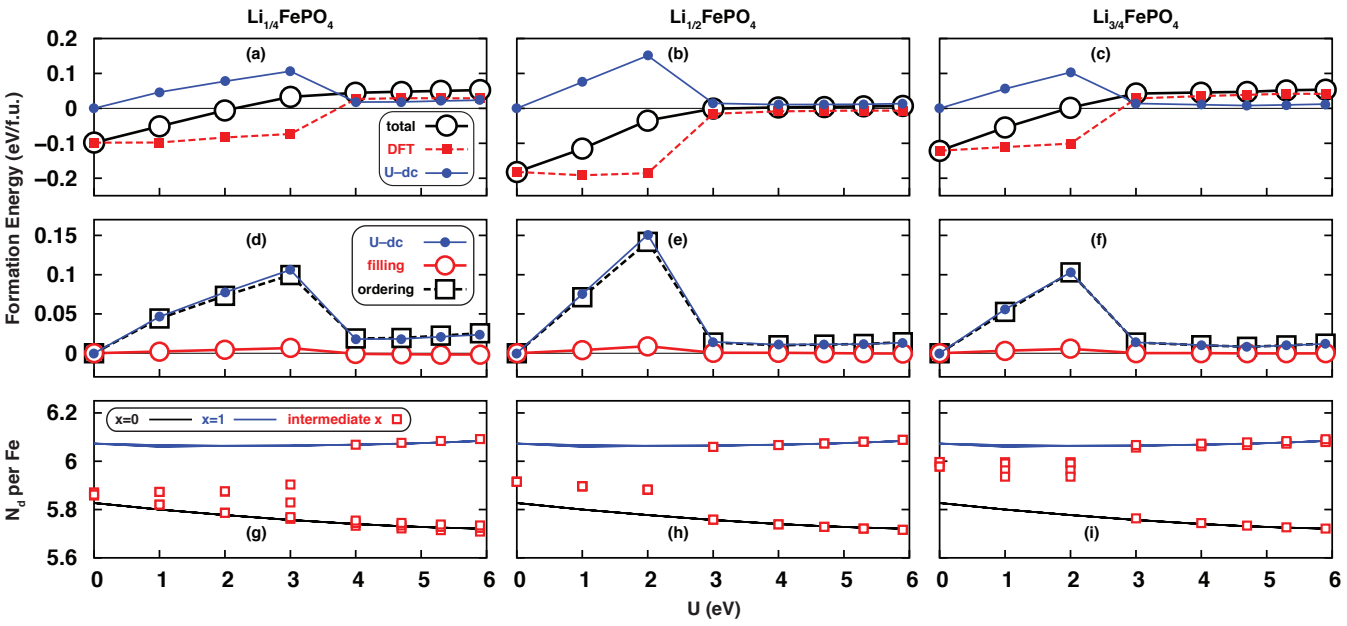

FIG. 12. Total Li_xFePO_4 formation energy (open black circles) and its DFT (filled red squares) and U–dc (filled blue circles) components as a function of U for (a) $x = 1/4$, (b), $1/2$, and (c) $x = 3/4$. (d)–(f) show the corresponding plots of Li_xFePO_4 U–dc (filled blue circles) formation energy component and its orbital filling (open red circles) and orbital ordering (open black squares) components as a function of U. (g)–(i) show the corresponding plots of number of d electrons per Fe as a function of U for $FePO_4$ (black line), Li_xFePO_4 (open red squares), and $LiFePO_4$ (blue line). All data correspond to the case of relaxed structures.

terpolation of endmember values are negligible. σ^2 gradually increases with U and the values for intermediate x always lag behind the endmember linear interpolation; the effect is substantially dampened but not entirely eliminated when CO increases σ^2 for intermediate x. We note that with structural relaxations after CO the σ^2 versus x curves are nearly linear, which illustrates that relaxations provide a further dampening of the general tendency towards phase separation with U stemming from the ordering term.

G. Phase stability of Li_xCoPO_4

To further validate our general understanding of the impact of U on phase stability, we investigate Li_xCoPO_4. This material is isostructural to the olivine Li_xFePO_4 structure shown in Fig. 1 with (nominally) an additional electron on the transition metal site. Li_xCoPO_4 is of interest since it has been shown to have a very high voltage (4.8 V) as a cathode material.[84] It is intriguing physically since unlike Li_xFePO_4 it does have a stable intermediate compound, for $x \approx 2/3$.[85–87]

We consider the lowest-energy configuration of $Li_{2/3}CoPO_4$ deduced by Strobridge *et al.*[87] and study the formation energy as a function of U with the frozen $U = 0$ structures. Experimentally the Li_xCoPO_4 system is AFM,[86,88] so our calculations consider the endmembers in the AFM state. We base our calculations on the magnetic configuration of $LiCoPO_4$, which is identical to that of $LiFePO_4$.[72,88] For $Li_{2/3}CoPO_4$ we find the AFM state to be unstable and devolves into a ferrimagnetic state. In this state one of the Co sites has no magnetic moment unlike the $\pm \approx 2.6 - 2.7\ \mu_B$ values of the other 11 leading to a total magnetization of $\approx 3.2\mu_B$.

We find total formation energies of -0.18, -0.14, and -0.03 eV for U values of 0, 2, and 5.48 eV, respectively. This corresponds to the same trend of formation energy increasing with U. We again find the positive formation energy contribution is the U–dc component, and here also the filling contribution is very small (magnitude of at most 20 meV) so the origin is increased ordering of the endmember d states relative to those of the intermediate x species.

For the above analysis we have restricted our attention to the AFM or AFM-like states as they are the experimental magnetic structure for Li_xCoPO_4. However, we note that the magnetic ground state of Li_xCoPO_4 predicted by DFT+U changes as a function of U, which is likely the origin of a previous study finding the formation energy becomes more negative as a function of U.[87] For $LiCoPO_4$ we find a ferromagnetic (FM) ground state within DFT with the AFM state 37 meV higher in energy, whereas for $CoPO_4$ we find a non-spin-polarized (NSP) ground state with the FM and AFM states 57–61 meV higher in energy. At $U = 2$ the ground state

of $LiCoPO_4$ becomes antiferromagnetic, and by $U = 5.5$ eV the ground state for both endmembers is AFM consistent with experiments. For $x = 2/3$ we find the FM state is unstable within DFT and the NSP state is 0.54 eV higher in energy than the ferrimagnetic state. At $U = 2$ eV the FM state becomes metastable only 7 meV above the ferrimagnetic state, and for $U = 5.5$ eV the FM state becomes the ground state with the ferrimagnetic state 68 meV high in energy. In any case, DFT+U does predict the $x = 2/3$ phase to be stable, qualitatively consistent with experiment.

H. Impact of double counting on phase separation trend

Our preceding analysis shows that it is valuable to recast the U–dc energy as the sum of ordering and filling terms, as the filling term was shown to have negligible impact on formation energies. However, there is still utility in analyzing what can be learned by separately inspecting E_U and $E_{\rm dc}$, given that the E_U term specifically is handled much more precisely in the context of DFT+DMFT.

The simplest possible explanation for the positive U–dc formation energy contribution comes from the form of the dc term Eq. 4. We expect the Li in Li_xCoO_2 and other intercalation materials will be ionized and donate some amount of charge (depending on the degree of hybridization with O p states) to Co. Therefore, we might make the assumption that N_d is linear in x. Since energy contributions linear in x do not contribute to the formation energy by the definition of Eq. 13, this means the term linear in N_d in the dc term cannot contribute to the formation energy. The other part of the dc, however, yields a term proportional to $-N_d^2$ (a negative quadratic in N_d) in the total energy. With the assumption of a linear relationship between N_d and x, this term is a negative quadratic in x that necessarily provides a positive formation energy contribution.

This simple kind of argument fails to fully describe the observed behavior for the following reasons, which we illustrate using the simplest example of $Li_{1/2}CoO_2$ without CO considering the frozen $U = 0$ structures. The first two reasons come from the fact that the variation of N_d with x is in fact substantially nonlinear, as can be easily seen for the $U > 1$ eV data in Fig. 5(c). In this regime, N_d for $x = 1/2$ is much closer to the $x = 1$ value than the $x = 0$ value. For example, for $U = 5$ eV the N_d values are 7.19, 7.28, and 7.30 for $x = 0$, $x = 1/2$, and $x = 1$, respectively. First of all, this means that the contribution of the dc energy that is proportional to N_d will contribute to the formation energy. For example, for this case it takes on the value of +89 meV for $U = 5$ eV.

Secondly, the quadratic part of the dc energy no longer necessarily gives a positive formation energy contribution for N_d that is nonlinear in x. One can parametrize the deviation from linearity using the additive form $N_d(x) = \overline{N_d(x)} + \delta_x$, where $N_d(x)$ is the N_d value for Li concentration x, $\overline{N_d(x)} = (1-x)N_d(0) + xN_d(1)$ is the linear value of $N_d(x)$, and δ_x is the deviation from linearity. Here we assume a single site for clarity. It then can be shown that the formation energy contribution stemming from the quadratic part of the dc energy is

$$FE_{\rm dc}^{\rm quad}(x) = \frac{1}{2}U\Big\{x(1-x)\left[N_d(1) - N_d(0)\right]^2 - 2\overline{N_d(x)}\delta_x\left(1 + \frac{\delta_x}{2\overline{N_d(x)}}\right)\Big\}. \quad (15)$$

Note that the term proportional to δ_x^2 can be ignored as δ_x should be much smaller than $2\overline{N_d(x)}$. When $\delta_x = 0$ (N_d is linear with x), we indeed have a positive formation energy contribution since the second term vanishes and the first term will be positive since $N_d(0) \neq N_d(1)$. However, this second term can lead to a significant negative (phase stabilizing) formation energy contribution when δ_x is positive and non-negligible. This actually results in a strongly negative formation energy contribution in the present case: for $U = 5$ eV, for example, the formation energy contribution from the quadratic part of the dc is -1.29 eV. Therefore, the dc term is not responsible for driving phase separation in this regime of U.

The third and final reason the simple argument fails is that the E_U term also contributes significantly to the formation energy. For example, for $U = 5$ eV the formation energy contribution from the interaction term is +1.78 eV, strongly driving phase separation.

Additionally, even in the limit of small U, in which the dc does provide a phase separation contribution, it is not fully responsible for the overall trend. In this limit, the impact of U on the interaction and dc formation energy components depends solely on the DFT density matrix. Computing $\partial E_U/\partial U$ and $-\partial E_{dc}/\partial U$ from Eqns. 3 and 4, respectively, and evaluating them at $U = 0$, we find that the dc energy contributes 7×10^{-3} and the interaction energy contributes a larger 13×10^{-3} to the change in total formation energy.

I. Average intercalation voltage of Li_xCoO_2 and Li_xFePO_4

Up to now our analysis of the DFT+U energetics has focused on the formation energy, and we seek other observables to probe the fidelity of our total energy calculations. Therefore, we now turn to average intercalation voltage, which is a function of the energy difference of the cathode endmembers and the energy of bulk Li (see Eq. 14) and can be measured experimentally.

Figure 13 shows the behavior of the average intercalation voltage as a function of U. As found previously, the voltages tend to increase with U for both Li_xCoO_2 and Li_xFePO_4.[78] For Li_xCoO_2 using relaxed structures, the computed voltage exhibits one discontinuity at $U = 2$ eV

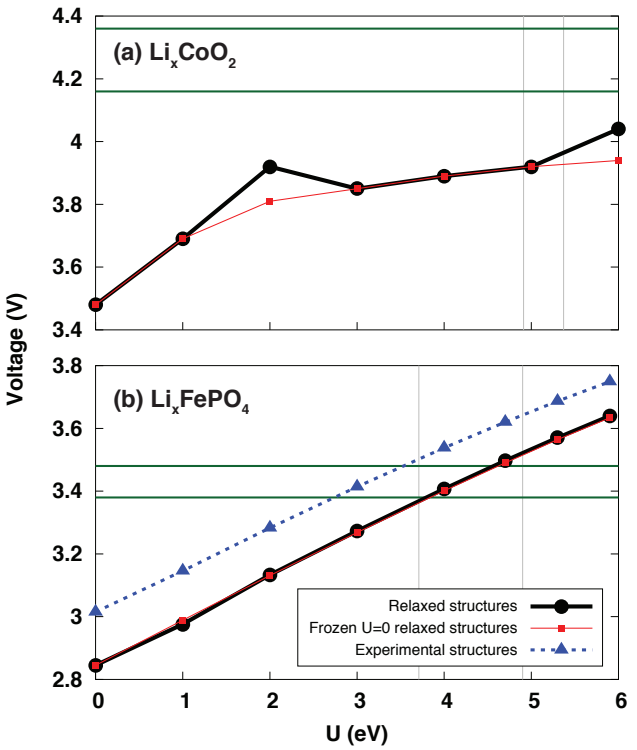

FIG. 13. Average intercalation voltage of (a) Li_xCoO_2 and (b) Li_xFePO_4 as a function of U shown using relaxed structures and frozen $U = 0$ relaxed structures. For Li_xFePO_4 the results using the experimental structures are also shown. Green lines indicate the range of the average voltage measured from experiment, and grey lines indicate U values of the endmembers computed via the linear response method.[78]

after which CoO_2 gaps and another at $U = 5$ eV after which $LiCoO_2$ becomes high spin. Otherwise, the values are almost identical to those found using the frozen $U = 0$ structures. The DFT value is 3.48 V and there is an increase to 3.92 V at $U = 5$ eV. We note that the predicted voltages for Li_xCoO_2 are smaller than those reported in the work of Zhou *et al.*,[78] but agree with several more recent studies.[27,28,89] Ultimately, DFT+U underpredicts the average voltage of Li_xCoO_2 compared to the experimental value of 4.26 V.[65] For Li_xFePO_4 using relaxed structures, the DFT voltage is 2.85 V and increases approximately linearly to 3.50 V at $U = 4.7$ eV, in agreement with the experimental voltage of 3.43 V.[20,90] Using the experimental structures, the predicted intercalation voltage is enhanced by 0.1-0.2 V.

In Li_xFePO_4, the two endmembers have similar properties as they are AFM insulators with very well localized electronic states. Therefore, it is possible that DFT+U is effective at describing the energetics of both phases and hence can capture the voltage effectively. However, in Li_xCoO_2 one endmember ($LiCoO_2$) is a band insulator while the other is a Fermi liquid (in experiment); the latter is found to be a magnetic metal or insulator within DFT+U depending on U. We speculate that the distinct nature of the endmembers for Li_xCoO_2, and their inadequate description within DFT+U, will lead DFT+U to make energetic errors which vary substantially for the different endmembers causing a worse description of the voltage as compared to the olivines. A forthcoming DFT+DMFT study will address this issue.

J. Li order-disorder transition temperature of $Li_{1/2}CoO_2$

Another observable with which we can assess the accuracy of DFT+U energetics, albeit at a fixed composition, is the order-disorder (O-D) transition temperature for Li. This is the temperature above which the Li ions and vacancies become disordered. Here we consider $Li_{1/2}CoO_2$, whose experimental O-D temperature is 333 K.[16]

We estimate the O-D transition temperature based on the ground state total energies of the ordered and disordered (SQS) phases using the equation

$$T_{\mathrm{O-D}} = \frac{E_D - E_O}{k_B \ln(2)},$$

where k_B is the Boltzmann constant and the factor of $\ln(2)$ comes from the entropy of mixing for $x = 1/2$. This expression is an approximation to performing finite-temperature Monte Carlo simulations on a cluster expansion based on such ground-state total energies. Past work suggests that this simpler expression should reasonably capture trends in $T_{\mathrm{O-D}}$.[91–94] Performing a cluster expansion of Li_xCoO_2 using DFT+U would likely be formidable given the many spurious ordered states which form at nonstochiometric compositions, as will be elucidated below.

Our predicted $T_{\mathrm{O-D}}$ for an optimal 42-ion SQS cell frozen to the relaxed $U = 0$ structures is illustrated in Fig. 14(a). Here within DFT the temperature is overestimated by around 25 K with respect to the experimental value. For small values of U the temperature decreases by as much as 32 K, bringing the prediction closer to the experimental value. However, for $U > 2$ eV, there is a very rapid increase in the predicted transition temperature to values of around 500–600 K, nearly a factor of two greater than the experimental value.

The Co magnetic moments and N_d values as a function of U are shown in panels (b) and (c) of Fig. 14, respectively. For small U there are small deviations of the magnetic moments and N_d compared to those of the ordered structure due to the different local environments of the Co in the disordered phase. The range of these values are enhanced for $U = 2$ eV, above which both the ordered and disordered cells charge order and open an electronic band gap [see panel (d)]. After the CO transition, there is still some spread in the magnetic moment and N_d values for the disordered phase with respect to those of the ordered phase. In this particular case, structural relaxations actually amplify these trends, resulting

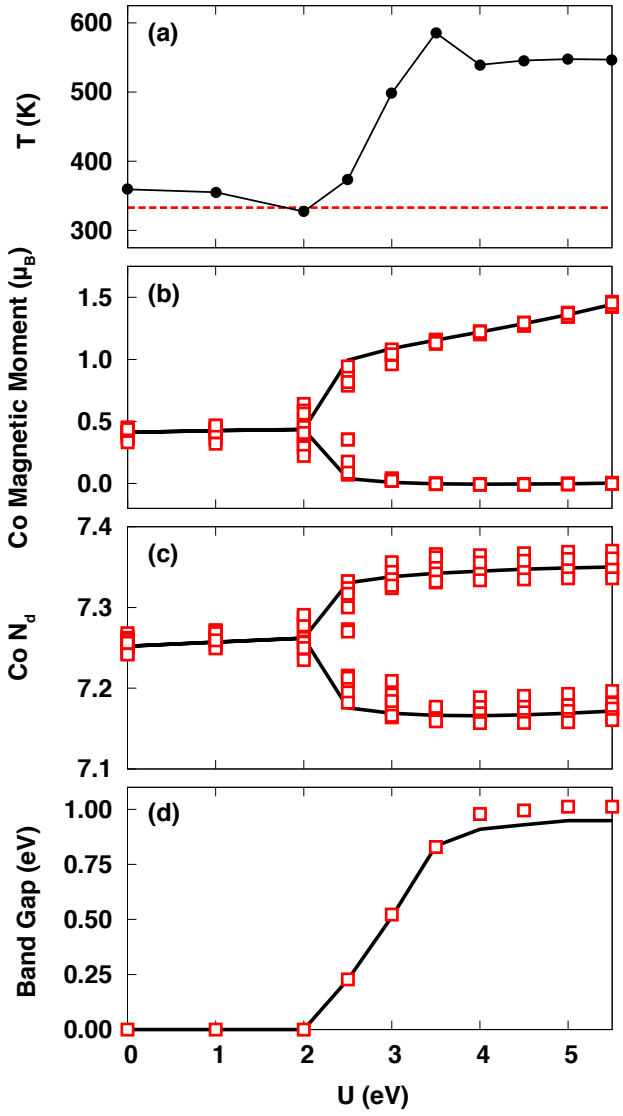

FIG. 14. (a) Li order-disorder transition temperature, (b) Co magnetic moments, (c) Co N_d, and (d) band gap for $Li_{1/2}CoO_2$ as a function of U using the frozen $U = 0$ eV structures. The disordered phase is modeled by an optimal 42-ion special quasirandom structure. In panel (a) the horizontal red line indicates the experimental order-disorder transition temperature from Ref. 16. For the other panels black lines (red squares) correspond to results from the ordered (disordered) structure.

in a substantially higher T_{O-D} for $U = 4$ eV, for example (see Supplementary Material for more details).

This demonstrates that the CO transition found within the DFT+U approach is largely responsible for the erratic behavior of the predicted Li order-disorder transition temperature for $Li_{1/2}CoO_2$. In the Supplementary Material, we show results for additional SQS cells with and without structural relaxations. We find that within DFT T_{O-D} can be overestimated or underestimated depending on the particular cell. A substantial increase in T_{O-D} due to CO is often observed, though it is not always as dramatic this particular case and does not always lead to as large a disagreement with the experimental value. In general, the results indicate that DFT+U is highly unreliable in predicting the order-disorder transition temperature due to CO. This further supports the notion that CO is an artifact of the approximate nature of the interaction in DFT+U, consistent with the fact that it is not observed in experiment. While spurious CO appears to be essential for properly attaining a phase stable system in $Li_{1/2}CoO_2$, as discussed in Sec. IV C, it appears to cause severe problems in the SQS supercell. While it is possible that more reasonable behavior emerges for substantially larger SQS supercells, which would be computationally expensive, this is beyond the scope of the current paper.

It should be noted that the spurious behavior we have documented in the context of this SQS calculation of T_{O-D} would likely manifest itself in any parameterization of the cluster expansion. In the best case scenario, this could lead to a complicated cluster expansion with long range interactions. The entire procedure could become ill-posed in the worst case with numerous orbitally ordered and/or CO states close in energy for a given Li ordering. This behavior does not bode well for the application of DFT+U in alloy thermodynamics. Given that DFT+DMFT does not necessitate charge/orbital ordering in order to capture the energetics of strongly correlated systems, it is likely not to share these deficiencies.

V. CONCLUSIONS

At the DFT+U level of theory, the on-site U tends to destabilize intermediate-x compounds of both phase stable Li_xCoO_2 and phase separating Li_xFePO_4, though qualitatively correct results are obtained for formation energies in both cases for physically reasonable values of U. A new formation energy decomposition, which disentangles the distinct roles of the filling and ordering of d orbitals, reveals that reduced orbital ordering in compounds of intermediate Li concentration relative to the endmembers is responsible for this effect. For intermediate x DFT+U predicts charge ordering which opens electronic band gaps and dampens, though does not eliminate, the tendency for phase separation. While charge ordering and an appreciable band gap are spurious for $Li_{1/2}CoO_2$, charge ordering is essential for retaining a phase stable system, as found in experiment, at reasonable values of U. This deficiency appears to be a manifestation of the Hartree-Fock treatment of the interaction energy within DFT+U, whereby static ordering is required to properly capture the energetics of strong electronic correlations. Indeed, it is demonstrated that the origin of the charge ordering arises from interaction energy within DFT+U, as opposed to the double counting correction. Structural relaxations, which similarly

only reduce the magnitude of the U-induced destabilization of intermediate compositions, have a more significant impact on Li_xFePO_4 than Li_xCoO_2 due to the stronger electron-lattice coupling. The same generic formation energy behavior is observed in Li_xCoPO_4, for which experiment dictates that a stable intermediate-x compound exists unlike for isostructural Li_xFePO_4.

The Li order-disorder transition temperature of $Li_{1/2}CoO_2$ behaves erratically when computed using SQS supercells within DFT+U as a result of charge ordering; severe overestimations are not uncommon. Along with a lack of experimental evidence and the induction of a spurious insulating state, this further supports the notion that static charge ordering is likely an unphysical artifact of the method. Future work should focus on improved methods for predicting total energies in realistic correlated electron materials using dynamical mean-field theory or other approaches. Given that many of the deficiencies that we have identified in this study appear to be associated with the Hartree-Fock treatment of the interaction energy within DFT+U, it is likely that DFT+DMFT could offer substantial improvements.

ACKNOWLEDGMENTS

This research used resources of the National Energy Research Scientific Computing Center, a DOE Office of Science User Facility supported by the Office of Science of the U.S. Department of Energy under Contract No. DE-AC02-05CH11231. E.B.I. gratefully acknowledges support from the U.S. Department of Energy Computational Science Graduate Fellowship (Grant No. DE-FG02-97ER25308).

* eric.isaacs@columbia.edu
† chris.marianetti@columbia.edu

[1] P. Hohenberg and W. Kohn, Phys. Rev. **136**, B864 (1964).
[2] W. Kohn and L. J. Sham, Phys. Rev. **140**, A1133 (1965).
[3] G. Kotliar and D. Vollhardt, Phys. Today **57**, 53 (2004).
[4] E. Morosan, D. Natelson, A. H. Nevidomskyy, and Q. Si, Adv. Mater. **24**, 4896 (2012).
[5] N. F. Mott, Rev. Mod. Phys. **40**, 677 (1968).
[6] M. Imada, A. Fujimori, and Y. Tokura, Rev. Mod. Phys. **70**, 1039 (1998).
[7] J. G. Bednorz and K. A. Müller, Z. Phys. B **64**, 189 (1986).
[8] A. P. Ramirez, J. Phys.: Condens. Matter **9**, 8171 (1997).
[9] P. Coleman, in *Handbook of Magnetism and Advanced Magnetic Materials* (John Wiley & Sons, Ltd., 2007).
[10] R. O. Jones and O. Gunnarsson, Rev. Mod. Phys. **61**, 689 (1989).
[11] R. Jones, Rev. Mod. Phys. **87**, 897 (2015).
[12] G. Kotliar, S. Y. Savrasov, K. Haule, V. S. Oudovenko, O. Parcollet, and C. A. Marianetti, Rev. Mod. Phys. **78**, 865 (2006).
[13] V. I. Anisimov, F. Aryasetiawan, and A. I. Lichtenstein, J. Phys. Condens. Matter **9**, 767 (1997).
[14] K. Momma and F. Izumi, J. Appl. Crystallogr. **44**, 1272 (2011).
[15] K. Mizushima, P. Jones, P. Wiseman, and J. Goodenough, Mater. Res. Bull. **15**, 783 (1980).
[16] J. N. Reimers and J. R. Dahn, J. Electrochem. Soc. **139**, 2091 (1992).
[17] A. Van der Ven, M. K. Aydinol, G. Ceder, G. Kresse, and J. Hafner, Phys. Rev. B **58**, 2975 (1998).
[18] C. Wolverton and A. Zunger, Phys. Rev. Lett. **81**, 606 (1998).
[19] A. K. Padhi, K. S. Nanjundaswamy, and J. B. Goodenough, J. Electrochem. Soc. **144**, 1188 (1997).
[20] A. K. Padhi, K. S. Nanjundaswamy, and J. B. Goodenough, J. Electrochem. Soc. **144**, 1609 (1997).
[21] C. Delacourt, P. Poizot, J.-M. Tarascon, and C. Masquelier, Nat. Mater. **4**, 254 (2005).
[22] J. L. Dodd, R. Yazami, and B. Fultz, Electrochem. Solid-State Lett. **9**, A151 (2006).
[23] F. Zhou, C. A. Marianetti, M. Cococcioni, D. Morgan, and G. Ceder, Phys. Rev. B **69**, 201101 (2004).
[24] S. P. Ong, V. L. Chevrier, and G. Ceder, Phys. Rev. B **83**, 075112 (2011).
[25] F. Zhou, T. Maxisch, and G. Ceder, Phys. Rev. Lett. **97**, 155704 (2006).
[26] B. Andriyevsky, K. Doll, and T. Jacob, Phys. Chem. Chem. Phys. (2014).
[27] M. Aykol and C. Wolverton, Phys. Rev. B **90**, 115105 (2014).
[28] M. Aykol, S. Kim, and C. Wolverton, J. Phys. Chem. C **119**, 19053 (2015).
[29] D.-H. Seo, A. Urban, and G. Ceder, Phys. Rev. B **92**, 115118 (2015).
[30] P. B. Visscher, Phys. Rev. B **10**, 943 (1974).
[31] M. Marder, N. Papanicolaou, and G. C. Psaltakis, Phys. Rev. B **41**, 6920 (1990).
[32] B. Himmetoglu, A. Floris, S. de Gironcoli, and M. Cococcioni, Int. J. Quant. Chem. **114**, 14 (2014).
[33] D. M. Ceperley and B. J. Alder, Phys. Rev. Lett. **45**, 566 (1980).
[34] S. H. Vosko, L. Wilk, and M. Nusair, Can. J. Phys. **58**, 1200 (1980).
[35] J. P. Perdew and A. Zunger, Phys. Rev. B **23**, 5048 (1981).
[36] J. P. Perdew and Y. Wang, Phys. Rev. B **45**, 13244 (1992).
[37] J. P. Perdew, J. A. Chevary, S. H. Vosko, K. A. Jackson, M. R. Pederson, D. J. Singh, and C. Fiolhais, Phys. Rev. B **46**, 6671 (1992).
[38] J. P. Perdew, K. Burke, and M. Ernzerhof, Phys. Rev. Lett. **77**, 3865 (1996).
[39] S. L. Dudarev, G. A. Botton, S. Y. Savrasov, C. J. Humphreys, and A. P. Sutton, Phys. Rev. B **57**, 1505 (1998).
[40] A. I. Liechtenstein, V. I. Anisimov, and J. Zaanen, Phys. Rev. B **52**, R5467 (1995).
[41] J. Chen, A. J. Millis, and C. A. Marianetti, Phys. Rev. B **91**, 241111 (2015).
[42] H. Park, A. J. Millis, and C. A. Marianetti, Phys. Rev. B **92**, 035146 (2015).
[43] J. P. Perdew, R. G. Parr, M. Levy, and J. L. Balduz, Phys. Rev. Lett. **49**, 1691 (1982).
[44] V. I. Anisimov, I. V. Solovyev, M. A. Korotin, M. T.

Czyyk, and G. A. Sawatzky, Phys. Rev. B **48**, 16929 (1993).
[45] M. Cococcioni and S. de Gironcoli, Phys. Rev. B **71**, 035105 (2005).
[46] E. Gull, A. J. Millis, A. I. Lichtenstein, A. N. Rubtsov, M. Troyer, and P. Werner, Rev. Mod. Phys. **83**, 349 (2011).
[47] K. Haule, Phys. Rev. B **75**, 155113 (2007).
[48] H. Park, A. J. Millis, and C. A. Marianetti, Phys. Rev. B **89**, 245133 (2014).
[49] H. Park, A. J. Millis, and C. A. Marianetti, Phys. Rev. B **90**, 235103 (2014).
[50] E. B. Isaacs and C. A. Marianetti, Phys. Rev. B **94**, 035120 (2016).
[51] M. K. Aydinol, A. F. Kohan, G. Ceder, K. Cho, and J. Joannopoulos, Phys. Rev. B **56**, 1354 (1997).
[52] G. Kresse and J. Hafner, Phys. Rev. B **49**, 14251 (1994).
[53] G. Kresse and J. Hafner, Phys. Rev. B **47**, 558 (1993).
[54] G. Kresse and J. Furthmüller, Phys. Rev. B **54**, 11169 (1996).
[55] G. Kresse and J. Furthmüller, Comput. Mater. Sci. **6**, 15 (1996).
[56] P. E. Blöchl, Phys. Rev. B **50**, 17953 (1994).
[57] G. Kresse and D. Joubert, Phys. Rev. B **59**, 1758 (1999).
[58] M. Methfessel and A. T. Paxton, Phys. Rev. B **40**, 3616 (1989).
[59] P. E. Blöchl, O. Jepsen, and O. K. Andersen, Phys. Rev. B **49**, 16223 (1994).
[60] A. Zunger, S.-H. Wei, L. G. Ferreira, and J. E. Bernard, Phys. Rev. Lett. **65**, 353 (1990).
[61] A. van de Walle, M. Asta, and G. Ceder, Calphad **26**, 539 (2002).
[62] A. van de Walle, Calphad **33**, 266 (2009).
[63] W. D. Johnston, R. R. Heikes, and D. Sestrich, J. Phys. Chem. Solids **7**, 1 (1958).
[64] H. J. Orman and P. J. Wiseman, Acta Crystallogr. Sect. C **40**, 12 (1984).
[65] G. G. Amatucci, J. M. Tarascon, and L. C. Klein, J. Electrochem. Soc. **143**, 1114 (1996).
[66] J. van Elp, J. L. Wieland, H. Eskes, P. Kuiper, G. A. Sawatzky, F. M. F. de Groot, and T. S. Turner, Phys. Rev. B **44**, 6090 (1991).
[67] M. Ménétrier, I. Saadoune, S. Levasseur, and C. Delmas, J. Mater. Chem. **9**, 1135 (1999).
[68] M. Ménétrier, D. Carlier, M. Blangero, and C. Delmas, Electrochem. Solid-State Lett. **11**, A179 (2008).
[69] C. de Vaulx, M.-H. Julien, C. Berthier, S. Hbert, V. Pralong, and A. Maignan, Phys. Rev. Lett. **98**, 246402 (2007).
[70] T. Motohashi, Y. Katsumata, T. Ono, R. Kanno, M. Karppinen, and H. Yamauchi, Chem. Mater. **19**, 5063 (2007).
[71] S. Kawasaki, T. Motohashi, K. Shimada, T. Ono, R. Kanno, M. Karppinen, H. Yamauchi, and G.-q. Zheng, Phys. Rev. B **79**, 220514 (2009).
[72] R. P. Santoro and R. E. Newnham, Acta Crystallogr. **22**, 344 (1967).
[73] G. Rousse, J. Rodriguez-Carvajal, S. Patoux, and C. Masquelier, Chem. Mater. **15**, 4082 (2003).
[74] P. Tang and N. A. W. Holzwarth, Phys. Rev. B **68**, 165107 (2003).
[75] S. Shi, C. Ouyang, Z. Xiong, L. Liu, Z. Wang, H. Li, D.-s. Wang, L. Chen, and X. Huang, Phys. Rev. B **71**, 144404 (2005).
[76] K. Zaghib, A. Mauger, J. B. Goodenough, F. Gendron, and C. M. Julien, Chem. Mater. **19**, 3740 (2007).
[77] F. Zhou, K. Kang, T. Maxisch, G. Ceder, and D. Morgan, Solid State Comm. **132**, 181 (2004).
[78] F. Zhou, M. Cococcioni, C. A. Marianetti, D. Morgan, and G. Ceder, Phys. Rev. B **70**, 235121 (2004).
[79] T. Motohashi, T. Ono, Y. Sugimoto, Y. Masubuchi, S. Kikkawa, R. Kanno, M. Karppinen, and H. Yamauchi, Phys. Rev. B **80**, 165114 (2009).
[80] K. Miyoshi, C. Iwai, H. Kondo, M. Miura, S. Nishigori, and J. Takeuchi, Phys. Rev. B **82**, 075113 (2010).
[81] T. Y. Ou-Yang, F.-T. Huang, G. J. Shu, W. L. Lee, M.-W. Chu, H. L. Liu, and F. C. Chou, Phys. Rev. B **85**, 035120 (2012).
[82] C. A. Marianetti, G. Kotliar, and G. Ceder, Phys. Rev. Lett. **92**, 196405 (2004).
[83] B. Ellis, L. K. Perry, D. H. Ryan, and L. F. Nazar, J. Am. Chem. Soc. **128**, 11416 (2006).
[84] K. Amine, H. Yasuda, and M. Yamachi, Electrochem. Solid-State Lett. **3**, 178 (2000).
[85] N. N. Bramnik, K. Nikolowski, C. Baehtz, K. G. Bramnik, and H. Ehrenberg, Chem. Mater. **19**, 908 (2007).
[86] H. Ehrenberg, N. N. Bramnik, A. Senyshyn, and H. Fuess, Solid State Sci. **11**, 18 (2009).
[87] F. C. Strobridge, R. J. Clment, M. Leskes, D. S. Middlemiss, O. J. Borkiewicz, K. M. Wiaderek, K. W. Chapman, P. J. Chupas, and C. P. Grey, Chem. Mater. **26**, 6193 (2014).
[88] R. P. Santoro, D. J. Segal, and R. E. Newnham, J. Phys. Chem. Solids **27**, 1192 (1966).
[89] V. L. Chevrier, S. P. Ong, R. Armiento, M. K. Y. Chan, and G. Ceder, Phys. Rev. B **82**, 075122 (2010).
[90] A. Yamada, S. C. Chung, and K. Hinokuma, J. Electrochem. Soc. **148**, A224 (2001).
[91] Z. W. Lu, D. B. Laks, S.-H. Wei, and A. Zunger, Phys. Rev. B **50**, 6642 (1994).
[92] C. Jiang, C. Wolverton, J. Sofo, L.-Q. Chen, and Z.-K. Liu, Phys. Rev. B **69**, 214202 (2004).
[93] C. Jiang, D. J. Sordelet, and B. Gleeson, Phys. Rev. B **72**, 184203 (2005).
[94] C. Jiang, C. R. Stanek, K. E. Sickafus, and B. P. Uberuaga, Phys. Rev. B **79**, 104203 (2009).